Kiloelectronvolt Particle-Induced Emission and Fragmentation of Polystyrene Molecules Adsorbed on Silver: Insights from Molecular Dynamics

A. Delcorte,[†] X. Vanden Eynde,[‡] P. Bertrand,[‡] J. C. Vickerman,[§] and B. J. Garrison*,[†]

Department of Chemistry, The Pennsylvania State University, 152 Davey Lab, University Park, Pennsylvania 16802, PCPM, Université Catholique de Louvain, 1 Croix du Sud, B1348 Louvain-la-Neuve, Belgium, and Surface Analysis Research Centre, Department of Chemistry, UMIST, P.O. Box 88, Manchester M60 1QD, U.K.

Received: October 5, 1999; In Final Form: December 22, 1999

Polystyrene oligomers adsorbed on Ag{111} have been used as a model system for a molecular dynamics study of polyatomic fragment ejection from large organic adsorbates on metals. The simulation of the interaction between the incident 500 eV Ar atoms and the sample predicts the nature and kinetic energy of the characteristic fragments observed in the low-mass range of the experimental polystyrene secondary ion mass spectrum (SIMS). This agreement confirms that characteristic molecular fragments can be the result of a collisional emission process. Moreover, the results indicate that the ejection of intact molecules occurs frequently. To understand the mechanisms of emission of fragments and parent molecules, a representative set of trajectories has been analyzed in detail. The ejection of characteristic fragments is primarily due to the direct interaction between the primary particle and the organic adsorbate. In contrast, desorption of intact molecules is induced by collision cascades in the sample surface. The emission of energetic intact molecules is best explained by a cooperative uplifting mechanism in which substrate atoms with similar momenta push the molecule upward. For comparison to the 500 eV bombardment conditions, simulations conducted with 5 keV primary particles show that large-scale simultaneous motions in the substrate may also occur, inducing the emission of many silver atoms and organic molecules in a single high action event.

1. Introduction

The bombardment of solid surfaces by kiloelectronvolt primary particles leads to a complex sequence of interactions which results in the sputtering (or desorption) of fragment, parent, and cluster ions or neutral molecules. The detection by appropriate mass spectrometers of the atomic and molecular ions sputtered by a low primary ion dose constitutes the basis of static secondary ion mass spectrometry (static SIMS).[1] Since its discovery 3 decades ago, the range of applications of SIMS has been continuously expanding, covering very diverse fields such as materials sciences, biotechnology, geology, and astronomy.[2] In particular, the emission of large, unfragmented molecules is a challenging issue in SIMS of organic and biological materials. The understanding of the very basic processes leading to the ejection of secondary species, and especially large molecular ions, has been hampered by the complexity of the microscopic phenomena.

From the experimental viewpoint, it is precarious to draw mechanistic conclusions with the experimental data provided by SIMS, because of the interference with ionization mechanisms. To overcome this limitation, the laser postionization of ejected neutrals appears to be a promising method when the competitive photofragmentation of the fragile organic molecules can be avoided. By this means, kinetic energy and angular distributions of neutral organic molecules have been obtained, elucidating the sputtering mechanisms for several systems.[3−5] The picture provided by these studies illustrates multiple processes, involving ballistic as well as thermal emission,[3,5] and shows an important dependence of the mechanisms on the organic molecule coverage.[4] Unfortunately, no report of this kind is available in the case of polymer fragments and, up to now, the investigated molecules have been limited in size. For larger molecules and polymer fragments, one must rely on the yields and kinetic energy distributions (KEDs) of sputtered ions.[6−14] Although the influence of ionization on the kinetic energy remains unclear in general, it has been demonstrated for C_xH_y ions sputtered from tricosenoic acid that the KEDs were independent of the charge state (positive versus negative) of the fragments.[9] It seems that, while ionization is a predominant factor to explain the observed ion *yields*, its effect on the fragment *energies* might be minor. Consequently, the kinetic energy of molecular ions allowed us to identify several emission processes, including the ballistic emission of small hydrocarbon precursor-like ions,[9] of faster and strongly dehydrogenated ions,[9,11] and of unexpectedly energetic cationized oligomers and molecules.[12] The periodic variation of the hydrocarbon ion kinetic energy was explained by a phenomenological model based on the concept of internal energy-dependent fragmentation of excited species, assuming a linear correlation between the kinetic and internal energies of the fragments.[15] Also, the weak effect of the primary ion nature, energy, and angle on the shape of the KEDs was evidenced.[14] Finally, the importance of metastable decay processes in the vacuum was demonstrated and interpreted with the formalism of the unimolecular reaction theory.[10,13]

In the theoretical context, advances have been hampered by the nature of the dynamics, involving mostly many-body

* To whom correspondence should be addressed. Phone: 1-(814)-863-2103. Fax: 1-(814)-863-5319. E-mail: bjg@psu.edu.
[†] The Pennsylvania State University.
[‡] Université Catholique de Louvain.
[§] UMIST.

10.1021/jp993539w CCC: $19.00
Published on Web 03/04/2000

interactions. Therefore, the successful application of analytical models has often been restricted to simple targets (elemental or oxide crystals) and to ejected atoms.[16] In parallel, molecular dynamics (MD) simulation has emerged as a powerful method to model kiloelectronvolt ion bombardment and sputtering of solids, including organic overlayers on inorganic substrates.[17] In early reports, it was shown that the ejection of intact benzene adsorbates could be induced by single or collective collision with substrate atoms, and a correlation between fragment size and kinetic energy was found.[18,19] The important effects of geometry and bonding state on the emission of intact molecules were highlighted.[18,20] Recently, the simulation of sputtering of aliphatic hydrocarbon chains showed that chemical reactions induced by the collision between moving organic fragments and molecules at rest were frequent, including hydrogen abstraction by hydrogen or methyl radicals.[21−24] Moreover, the SIMS spectra of alkanethiolate monolayers on gold were reasonably interpreted and, in particular, the formation of various gold thiolate clusters could be observed in the simulation.[25] The validity and power of the MD simulations have been further demonstrated by the remarkable agreement between measured and calculated energy and angular distributions for benzene adsorbates on silver.[26] In addition, the results obtained with polyatomic projectiles exemplify the predictive aspect of the method.[27−30] Interestingly, ref 29 indicates that phenyl rings weakly bound to a graphite surface can be softly ejected by an acoustic wave caused by the interaction with the fullerene projectile. To the best of our knowledge, the only report on the bombardment of polymers is due to Beardmore and Smith.[31] They bombarded a polyethylene crystal with 1 keV argon atoms and predicted the ejection of small hydrogen-deficient C_xH_y chain segments.

In this paper, MD simulations of 500 and 5 keV argon bombardment of polystyrene (PS) tetramers adsorbed on silver are presented. These simulations have been inspired by previous experimental studies of the sputtering of high molecular weight PS[10,11,13] and of PS oligomers under 15 keV ion bombardment.[12] In the latter work,[12] it has been shown that the emission of *intact* aromatic dibenzanthracene and tetraphenylnaphthalene molecules, as well as Ag-cationized PS oligomers, is undoubtedly collisional in nature. Although the experiments provide good clues concerning the emission processes of parentlike ions, they also show the need of a powerful model to unravel the details of the mechanisms. In addition, the positive ion mass spectrum of short PS oligomers adsorbed on Ag show all of the characteristic fragment peaks as observed for high molecular weight, bulk polystyrene. The kinetic energies of these fragments are close to those sputtered from high molecular weight polystyrene. Therefore, short PS oligomers adsorbed on a metal surface also seem to be a good model system to study the *fragmentation* of high molecular weight PS. The very distinctive fragmentation spectrum of PS, in contrast with polyethylene, constitutes a challenging feature to model, and the obtained results, if satisfactory, are thus expected to shed light on more complex fragmentation channels. Concerning the methodology, the ballistic nature of the ejection for both fragments and parentlike ions suggests that MD simulation is the appropriate choice. The primary particle energy in the MD simulation, 500 eV, has been mostly chosen to perform a large number of runs within a reasonable computation time. It appears low in comparison with SIMS experiments (15 keV), but previous studies have demonstrated that the emission mechanisms of small organic molecules and fragments are almost independent of the primary particle energy.[14,26] Nonetheless, a few trajectories are also calculated with 5 keV primary argon atoms in order to check the influence of the primary ion energy on the modeled mechanisms.

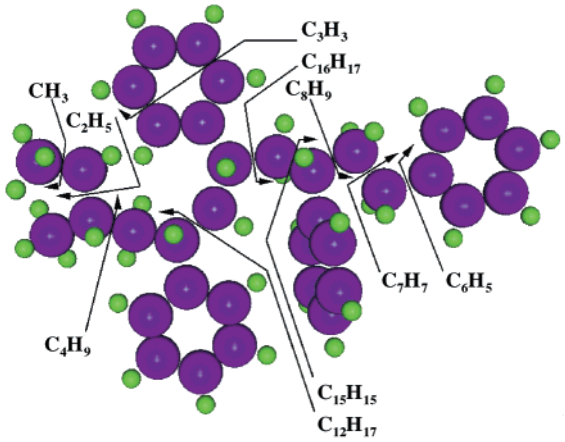

Figure 1. Picture of a *sec*-butyl-terminated PS tetramer. The characteristic fragments sputtered in the simulation are indicated by arrows. Of note is that the four pendant phenyls are equivalent.

2. Method

The Ar bombardment of *sec*-butyl-terminated polystyrene tetramers (Figure 1) adsorbed on a Ag(111) surface was modeled using MD computer simulations. The MD scheme has been described in extensive detail elsewhere.[32−36] Briefly, it consists of integrating Hamilton's equations of motion over some time interval to determine the position and velocity of each particle as a function of time. The energy and forces in the system are described by many-body interaction potentials. Experimentally observable properties, such as total yield, mass spectrum, kinetic energy, and angular distributions, are calculated from the final positions, velocities, and masses of all of the ejected species. Mechanistic information is obtained by monitoring the time evolution of relevant collisional events.

In the model, the silver substrate is approximated by a finite microcrystallite containing 1404 Ag atoms arranged in 9 layers of 156 atoms each. For the bombardment of PS tetramers by 500 eV argon atoms, five organic molecules (Figure 1) are placed on the Ag{111} surface, as shown in Figure 2. The entire system is quenched to a minimum energy configuration prior to Ar atom impact. Primary Ar atoms are directed along the surface normal. A total of 4000 Ar aiming points or trajectories directed within the impact area (rectangle in Figure 2) were calculated. Because of the larger size and disorder of the organic adsorbate as compared to previous studies,[25,26] the impact area should be close to the size of the crystal in order to sample the entire surface. Obviously, such an impact area would require a much larger crystal in order to provide a reasonable confinement of the collision cascades in the crystal and to avoid important edge effects. Instead, we define a central zone that includes both molecule and bare substrate. We feel this approximation is justified because the arrangement of PS tetramers on the Ag surface is not known experimentally.

Each trajectory is initiated using a fresh undamaged sample. The criterion for terminating the trajectory is that the total energy of any atom is too low to induce ejection. The termination times range from 0.5 to 6 ps, depending on the impact point of the primary particle and the manner in which the energy distributes within the solid. Open boundary conditions are used for the system.[33,35] That is, energetic particles that reach the sides or bottom of the computational cell are allowed to exit, taking their

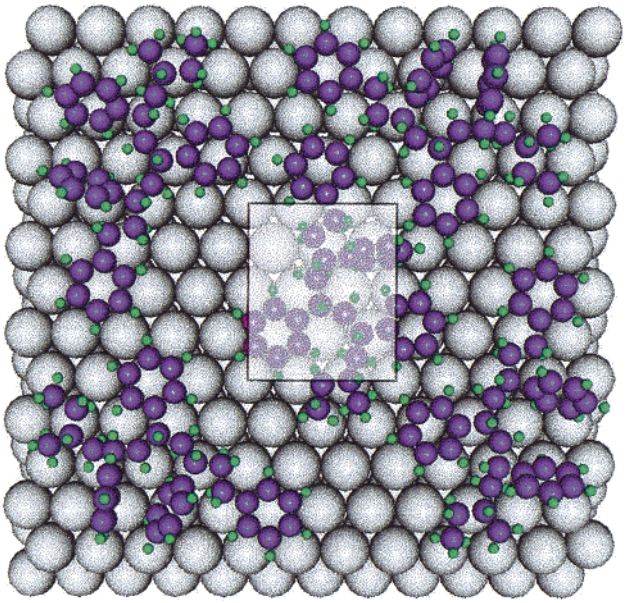

Figure 2. Surface configuration of the sample used for 500 eV Ar atom bombardment. Silver atoms are represented by large light gray spheres, carbon by dark purple spheres, and hydrogen by small light green spheres. The bombarded area is indicated by a shaded rectangle.

energy with them. In the real system, these energetic particles would transport energy into the regions of the solid further from the impact zone and not influence the ejection process. For the bombardment of PS tetramers by 5 keV argon atoms, a larger silver microcrystallite containing 6336 Ag atoms arranged in 12 layers of 528 atoms each is used. Thirteen PS molecules are placed on the Ag surface, in a similar configuration as the central molecule shown in Figure 2. Because of the large computer time requirement with this system, i.e., 5−10 h on one IBM-SP node per trajectory, only a hundred trajectories were calculated. In all of the considered systems, the mass of hydrogen was taken to be that of tritium (3 amu) to increase computational efficiency.[26] The mass of the PS tetramer is then 559 amu instead of 474 amu. To compare with experimental spectra, however, the mass of hydrogen is considered to be equal to 1 in the plots and discussion.

The blend of empirical pairwise and many-body potential energy functions used to represent the forces among the various atoms has been described in detail elsewhere.[26] Briefly, we use a purely repulsive Moliere potential to describe all interactions between the Ar and other atoms. This assumption is based on the fact that the Ar atom primarily imparts energy and momentum to the system and does not play a direct role in the chemistry of the bombardment process. For the remainder of the system, both the repulsive and attractive interactions are evaluated using many-body and pairwise potential functions. The Ag−Ag interactions are described by the MD/Monte Carlo corrected effective medium (MD/MC-CEM) potential function for fcc metals.[37−39] One attractive feature of the MD/MC-CEM potential is that it shows reasonable Coulombic behavior at small internuclear separation. The hydrocarbon interactions are described by the Brenner potential function.[40,41] This potential was fit to the energetics and structures of small hydrocarbon molecules, including radicals as well as graphite and diamond lattices. It allows for chemical reaction and accompanying changes in atomic hybridization during the course of a reaction. It is important to note that this hydrocarbon potential is confined only to short-range interactions of nearest neighbors and that long-range van der Waals type interactions are not included. As described in ref 23, a Moliere function is attached to the repulsive wall of the Brenner potential in order to handle high-energy collisions. For the sake of consistency with previous work,[26] the interactions for Ag−C and Ag−H are described by pairwise additive, Lennard-Jones potential functions. The Lennard-Jones parameters are chosen to obtain a reasonable binding energy for benzene molecules adsorbed on the silver surface. The Ag−C and Ag−H equilibrium distances of 2.3 Å were taken from an estimate for the height of benzene molecules above the Ag{111} surface,[42,43] and the energy well depth for the Ag−C and Ag−H interactions are respectively equal to 0.05 and 0.0083 eV. With these parameters, the binding energy of one PS tetramer to the silver substrate is ∼2.3 eV.

At the end of each simulation, the atoms, clusters, and molecules which have velocities directed away from the surface and are at a height of 6 Å above the original sample are regarded as ejected. For identifying clusters, pairs of atoms are checked to see if there is an attractive interaction between them, in which case they are considered linked.[32,44,45] A network of linked pairs is constructed, and the total internal energy of the group is evaluated. If the total internal energy is less than zero, then the group of atoms is considered to be an ejected molecule. This procedure, of course, overestimates the number of bound ejected molecules because some of these aggregates may have sufficient internal energy to decay unimolecularly during the flight to the detector.[45] This point is discussed in detail in the Results and Discussion section.

3. Results and Discussion

The SIMS spectrum is the result of the combined action of several processes, including collision cascades, fragmentation in the surface region, ionization, and metastable decay in the vacuum. Although current MD simulations cannot account for ionization processes and long-lifetime metastable decay, it is seen in the following discussion that the comparison between calculated and experimental results yields insights concerning these processes. Most of the results presented hereafter relate to the simulations performed with 500 eV Ar atoms. We first show how the very different time scale of the simulation, and its influence on the relative fraction of stable and reorganized species, can help to understand some features of the spectra (section 3.1). On the basis of unimolecular reaction theory, it is shown that the use of an internal energy filter, excluding highly excited fragments, provides a means to obtain better agreement with the experiment. The corrected mass spectrum is compared to the SIMS spectrum of short PS oligomers (section 3.2.). To go further into the comparison with experiment, the experimental and calculated energy distributions are presented in section 3.3. The good agreement with experiment allows us to present the detailed emission mechanisms of fragments and intact molecules provided by the time evolution of the trajectories (section 3.4). Because the primary particle energy might have an influence on the emission processes, the results obtained with 500 eV argon atoms are compared to 5 keV bombardment (section 3.5). Finally, the body of evidence provided by the simulation results in this paper and in previous work is summarized, suggesting a path toward a comprehensive view of thin organic layer sputtering.

The calculated mass spectrum is used as a road map for the analysis of the emission of organic species from PS oligomers (Figure 3). It is obtained by summing up the sputtered particles counted over the 4000 trajectories and sorting them as a function of their masses. In the spectrum of Figure 3a, no correction has been taken to account for ionization probabilities, ion stabilities,

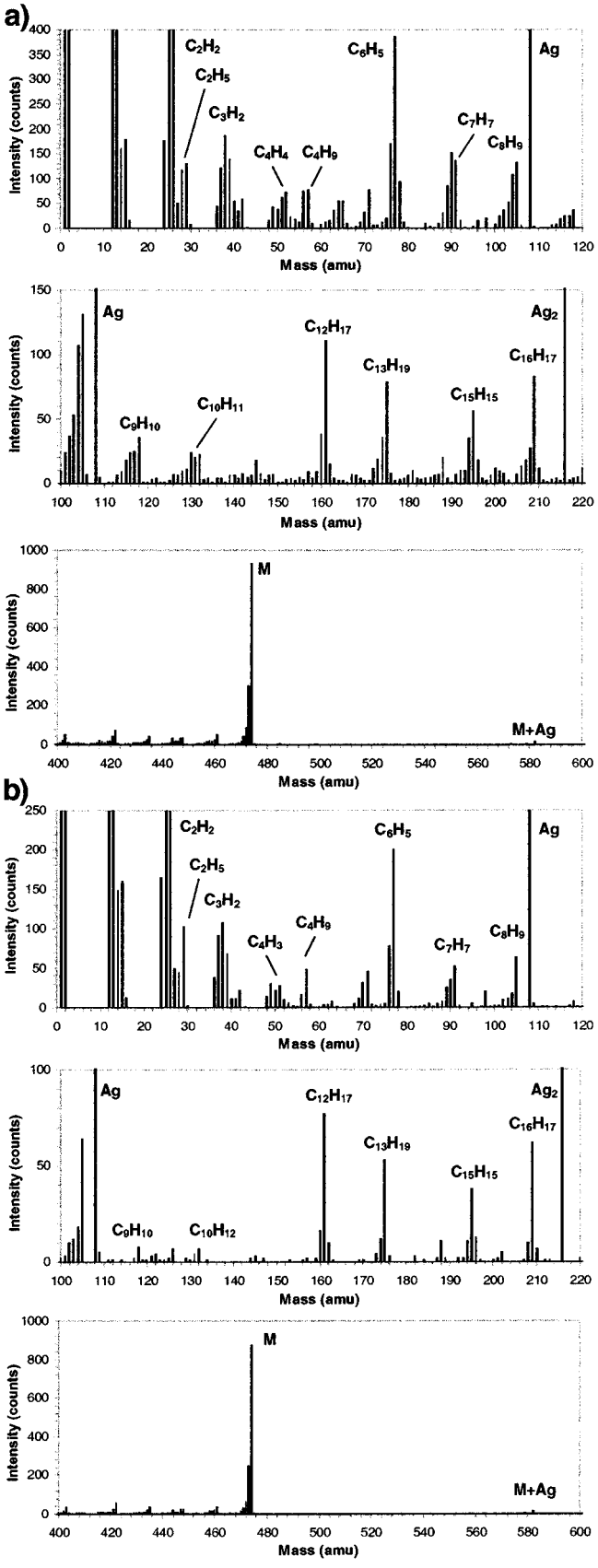

Figure 3. (a) Calculated mass spectrum of *sec*-butyl-terminated PS tetramers adsorbed on Ag{111} under 500 eV Ar atom bombardment, showing the species existing 6 ps after the primary particle impact. (b) Calculated internal energy resolved mass spectrum of the same sample. The spectrum excludes species sputtered with more internal energy than the calculated threshold for dissociation (see text). It does not *include* any product of unimolecular dissociation reactions.

TABLE 1: Daughter Fragments Produced by the Metastable Decay of 25 C_9H_9 Parent Species over a 100 ps Time scale

formula	mass (amu)	number	formula	mass (amu)	number
H	1	14	C_6H_2	74	1
H_2	2	1	C_7H_3	87	1
C_2H	25	3	C_7H_5	89	4
C_2H_2	26	6	C_7H_6	90	2
C_2H_3	27	2	C_7H_7	91	4
C_2H_4	28	3	C_9H_7	115	1
C_3	36	1	C_9H_9	117	10
C_3H_5	41	1			

or late unimolecular dissociation in the vacuum. Besides Ag atoms and clusters, the organic peaks of the mass spectrum essentially belong to two different classes. In the upper mass range beyond 400 amu, the mass spectrum is dominated by parent (or parentlike) species, i.e., the entire tetramer and its Ag-cationized homologue. The rest of the mass spectrum contains small fragments and larger chain segments of PS tetramers. A detailed comparison of the calculated mass spectra of Figure 3a,b with a representative SIMS spectrum is presented in section 3.2 as a preliminary to the description of the emission mechanisms revealed by the MD. The distinction between *fragments* and *parent species* will be maintained in the discussion.

3.1. Internal Energy and Unimolecular Dissociation. *(a) Metastable decay reactions.* In addition to ionization, the different time scales may be an important factor to explain the difference between experiment and simulation. Indeed, the calculated mass spectrum of Figure 3a shows the secondary species that exist ~6 ps after the primary ion impact, whereas the detection setup of most secondary ion mass spectrometers counts the sputtered ions arriving tens of microseconds later. Within this 6 orders of magnitude time gap, internally excited molecular species dissociate with a rate that is a nonlinear function of their internal energy excess. Experiments have shown that such metastable decays could be observed for times longer than 1 ns.[13,46] Nevertheless, such reactions are also likely to occur for shorter times of $10^{-12}-10^{-9}$ s that are inaccessible to the experiment. Unfortunately, it is currently impossible to extend the simulations up to 1 ns for each of the sputtered particles. In addition, the Brenner hydrocarbon potential used to model the C−C and C−H interactions is not expected to provide a quantitative description of these decomposition reactions. Nevertheless, extended calculations were performed with a few sputtered species in order to get qualitative indications concerning the reorganization and elimination reactions. In particular, the evolutions of 25 sputtered C_9H_9 fragments were followed up to 100 ps. The more excited fragments undergo one or several dissociation reactions in the investigated time range. Table 1 shows the reaction products at the end of the calculation. Among these reactions, H loss is predominant, but H_2, C_2H, and C_2H_2 losses are also observed. Rearrangements including hydrogen exchange between neighbor C atoms and transition between six- and seven-membered rings occur in the simulation. Nonetheless, fragments with six-member rings remain dominant at the end of the simulation. After approximately 100 ps, a significant number of species with seven carbon atoms is formed, including C_7H_7. It is interesting to note that one bicyclic, idenyllium radical (C_9H_7) is also formed as a result of two successive H atom losses accompanied by a rearrangement to form a five-membered ring. Although these calculations provide only qualitative indications of what can occur, the nature of the observed reactions is consistent with the literature.[47−49]

Despite our lack of knowledge concerning the details of fast metastable decay reactions, a simple criterion based on the internal energy of the fragments can be developed to gain insight into the importance of these postemission fragmentation processes. Indeed, the unimolecular reaction theory indicates that the internal energy (vibration + rotation) of polyatomic species is the major parameter governing dissociation reactions.[48] According to the theory, the particles that have more internal energy than a well-defined threshold rearrange or decompose within a given time range. The application of this theory requires first a correct determination of the internal energy of the sputtered polyatomic species and, second, a realistic estimate of the internal energy threshold for dissociation. These issues are addressed in the next paragraphs.

(b) Internal Energy of the Sputtered Species. For each molecular species, the internal energy can be calculated using eq 1[23]

$$E_{\text{int}} = V(r_{ij}) + \text{KE}(r_{ij}) - V_{\text{eq}} \quad (1)$$

where $V(r_{ij})$ and $\text{KE}(r_{ij})$ are respectively the potential and kinetic energies of the atoms relative to the center of mass of the molecule at the end of the sputtering event and V_{eq} is the calculated equilibrium potential energy of the same molecule in the vacuum. For all of the fragments below 130 amu and the entire molecule, V_{eq} is calculated by relaxing the fragments in the vacuum until the minimum energy was reached. To calculate the equilibrium potential energy of large fragments, abundant and very diverse because of the size of the parent molecule, a different procedure is developed. The sum of the energy well depths of the corresponding atoms in the relaxed entire molecule is used as an estimate for V_{eq}. This calculation provides a significantly overestimated absolute value of V_{eq}, given that the atoms in the entire PS tetramer are all completely coordinated, which is rarely the case in the fragments. To correct this systematic error, we assume that the large fragments are mostly produced by a single C−C scission in the backbone. The fragments formed by this channel have one undercoordinated carbon. The corresponding reduction of the potential energy is approximated by half the potential energy difference between the ethane molecule and two methyl radicals, that is, by half the value of this C−C bond strength in the Brenner hydrocarbon potential. The final numbers have been compared to those obtained from relaxation in the vacuum for several fragments, and the error is always less than 1 eV.

(c) Internal Energy Threshold for Dissociation. To check the stability of a given molecule, its internal energy has to be compared to a realistic energy threshold for unimolecular dissociation. In previous papers, dissociation threshold values of 5 and 10 eV have been proposed for benzene[26] and biphenyl[27] molecules, respectively. Similar values can be derived from published results, using internal energy versus dissociation rates curves. Consider for instance the cases of benzene (78 amu),[50,51] naphthalene (128 amu),[49] and phenanthrene (278 amu),[49] which decay mostly by H atom loss reactions in the range of dissociation rates of interest. When the time of flight of the ejected species and the maximum energy required for the corresponding lifetime are known, it is easy to calculate the threshold energy, below which most of such secondary species should be detected in our ToF−SIMS. The result is that more than 90% of benzene ions will be detected if their internal energy does not exceed 4.6 eV. The thresholds are larger for naphthalene (7.0 eV) and phenanthrene (7.5−8.0 eV). These results taken from the literature confirm that the thresholds vary from one molecule to another in relation with their size. Because our concern is not a single molecule or fragment but a large range of hydrocarbons between 1 and 500 amu, the use of a single energy threshold would lead to unrealistic results. The correct calculation of the energy thresholds requires the application of the quantum RRKM theory, relying on statistical mechanics, and its detailed application to the wide range of hydrocarbon molecules considered here is outside the scope of this paper. Nevertheless, a reasonable approximation of the relation between internal energy (E_{int}) and lifetimes (τ) is provided by the classical RRK theory, in which the molecule is represented by a set of s oscillators.[52] In this treatment, the rate of dissociation, r, of the molecule, equal to the inverse of the average lifetime τ, is given by eq 2 where A is a proportionality constant ($A \approx 10^{13}$ s^{-1}), E_0 is the critical energy for dissociation, and s is the number of vibrational modes in the molecule. In general, the number of vibrational modes, s, is equal to $3n - 6$. However, the comparison with experimental data shows that the use of $s = 3n - 6$ in eq 2 leads to a systematic error.[52] Instead, using half the number of oscillators yields a good agreement with the experiment. The same convention is used hereafter.

$$r = 1/\tau = A(1 - E_0/E_{\text{int}})^{s-1} \quad (2)$$

In the following discussion and figures, it is considered that an ejected species is stable if its probability to reach the detector unfragmented is above 90%. Assuming the simple exponential decay of parent molecules with time described by the RRK theory, a 90% survival probability corresponds to an average lifetime τ of the species that is at least 10 times greater than its time of flight to the detector. Using this value of τ, i.e., 10 times the value of the fragment time of flight in eq 2, one readily obtains the corresponding internal energy E_{int} below which more than 90% of the ejected species survive until they reach the detector. This particular value of E_{int} constitutes the internal energy threshold for dissociation, depending on the size of the molecule through the number of vibrational modes s. With this convention, the vast majority of the species having *less* internal energy than the threshold (*more* than 90%) are stable from the viewpoint of the experiment. In practice, E_0 lies in the range 3.5−5 eV for most of the relevant hydrocarbon molecules. For simplicity, a constant value of 5 eV is used in the calculation.

In Figure 4, the internal energy, calculated with eq 1, is plotted as a function of the mass of the organic fragments and molecules sputtered from PS tetramers. The average internal energy excess increases with increasing fragment mass. Nevertheless, this augmentation is followed by the increase of the energy threshold for dissociation determined using eq 2 and taking into account the time of flight of the different fragments. Therefore, the corrected mass spectrum of Figure 3b is less intense, in general, but there is not a clear dependence of the relative intensity change on the mass of the sputtered species, in contrast with the use of a constant energy threshold.[25] For instance, with the RRK-based threshold, 58% of C_3H_2 (38 amu), 52% of C_6H_5 (77 amu), 49% of C_8H_9 (105 amu), and 69% of $C_{12}H_{17}$ (161 amu) are found cool enough to survive until the virtual detector. In the range 110−220 amu, many minor peaks are more strongly reduced (C_9H_9, $C_{10}H_{10}$) while the major fragments, $C_{12}H_{17}$ (161 amu), $C_{13}H_{19}$ (175 amu), $C_{15}H_{15}$ (195 amu), and $C_{16}H_{17}$ (209 amu), keep a significant intensity (see formulas in Figure 1). In comparison with other fragments beyond 400 amu, the entire molecules are, in general, more stable, probably because no covalent bond breaking is needed for their emission. Because of the relatively high threshold for dissociation of the entire PS tetramer (28 eV), the intensity of this peak in the corrected mass spectrum is not significantly reduced (94% of its initial value).

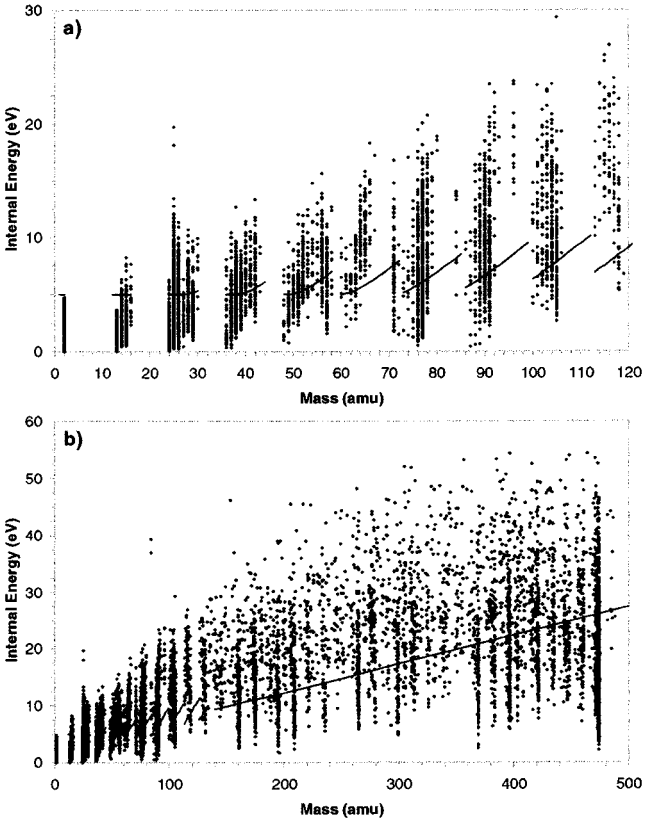

Figure 4. Scatter plot correlating the internal energies of the sputtered hydrocarbon fragments with their masses. Sputtered fragments are represented by black dots. The lines correspond to the calculated internal energy threshold for dissociation (see text). Only fragments below the threshold are considered as stable species.

Although the exact numbers change, using a slightly different value for E_0 (between 3.5 and 5 eV) does not modify the general trend described here. In addition, the exact value of the constant A does not significantly influence the results. A 1 order of magnitude increase or decrease of A does not modify the energy threshold by more than 10%. On the other hand, using the full number of oscillators s instead of $s/2$ in eq 2 leads to a 30−40% increase of the calculated energy thresholds, i.e., to a pronounced overestimation of the thresholds in comparison with the available data for benzene[50,51] and other aromatic compounds. [49]

3.2. Mass spectra. *(a) Experimental SIMS Spectrum.* In this section, the fragments and parent species sputtered in the simulation are compared to those observed in the SIMS experiment. For the simulation, *sec*-butyl-terminated PS tetramers are chosen as a model of both PS oligomers and high molecular weight PS. Indeed, it is assumed that the fragments with less than 10 carbon atoms, constituting the major part of the experimental SIMS spectra, do not require extensive rearrangement of longer chain segments to be formed. This assumption is confirmed by the positive SIMS spectrum of very low molecular weight PS shown in Figure 5. Except the high intensities of the fragments arising from the *sec*-butyl end group ($C_4H_9^+$ at 57 amu, $C_3H_5^+$ at 41 amu, and $C_2H_5^+$ at 29 amu) and from the H end group ($C_7H_7^+$ at 91 amu) shown in Figure 1 and despite the relative intensity differences, the nature of the sputtered ions is similar to the case of high molecular weight PS.[53] Before comparison of experiment and simulation results, it is worth noting that the enhancement of the chain end intensities in Figure 5 is not only due to the limited chain length but also due to the influence of the substrate. A "thick" sample

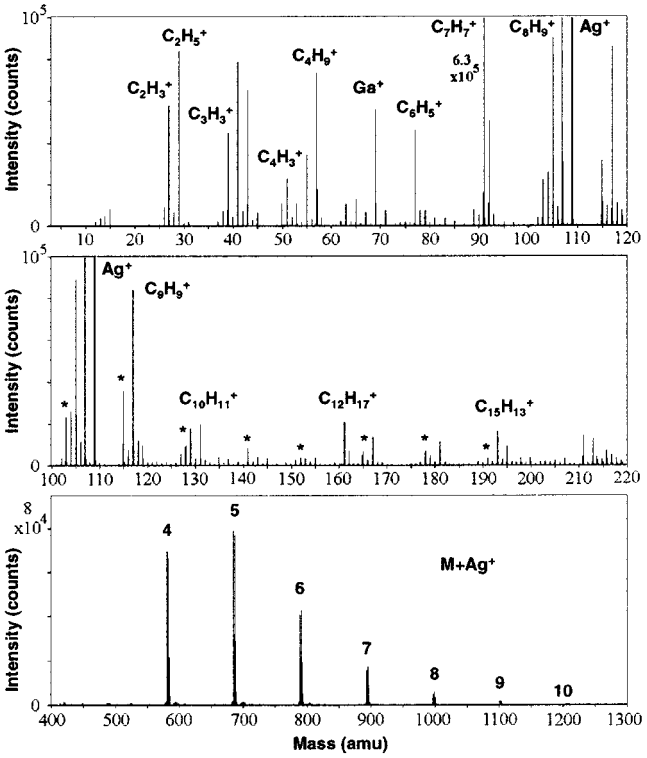

Figure 5. Experimental mass spectrum of *sec*-butyl-terminated PS oligomers adsorbed on a polycrystalline Ag foil. The intensity of $C_7H_7^+$, out of scale, is indicated on the left of the peak (top frame). The stars in the middle frame show the positions of polycyclic aromatic ions. The numbers in the bottom frame are the numbers of repeat units in the corresponding silver-cationized PS molecule.

of very low molecular weight PS does not show such a drastic relative increase of the chain end signals.[54] Being aware of these effects and of the current limitation of the MD code to model the sputtering of ionic species, our comparison of the experimental and calculated spectra is limited to the nature of the sputtered fragments.

Besides the intense chain end signature at 57 amu and the low mass fragments related to the butyl chain end (29, 41, and 43 amu), the experimental spectrum of PS oligomers in the low mass range is characteristic of the aromatic parts of the molecule, common with high molecular weight PS. Below 110 amu, unsaturated ions are observed, among which are the phenyl side group cation $C_6H_5^+$ (77 amu) and its fragments $C_3H_3^+$ (39 amu) and $C_4H_3^+$ (51 amu). Of note is that these fragments can arise from any of the phenyl side groups. In addition to the H end group whose influence is predominant in Figure 5, it must be mentioned that $C_7H_7^+$ (91 amu) and $C_8H_9^+$ (105 amu) are also characteristic of the interior of the chain, as indicated by the spectrum of high molecular weight PS and our simulation.

In the range 110−220 amu, the main fragments in the experiment are $C_9H_9^+$ (117 amu), $C_{10}H_9^+$ (129 amu), $C_{10}H_{11}^+$ (131 amu), $C_{12}H_{17}^+$ (161 amu), $C_{13}H_{11}^+$ (167 amu), $C_{14}H_{13}^+$ (181 amu), and $C_{15}H_{13}^+$ (193 amu). In contrast with smaller fragments, most of these peaks are characteristic of short oligomers and are not observed for high molecular weight PS. Instead, the intense peaks of the high molecular weight PS spectrum[10] in this mass range correspond to polycyclic aromatic ions (115, 128, 141, 152, 165, 178, and 191 amu; marked with a star in Figure 5). Polycyclic ions cannot be the result of a straightforward fragmentation of the chain involving only a few bond-breaking events. For these ions, complex fragmentation/rearrangement channels have been proposed in the literature.[55,56] Polycyclic aromatic ions are also present in the spectrum of

Figure 5, but they are not predominant. To explain the origin of the most intense peaks in this range of the PS oligomer spectrum, the influence of the chain ends must be invoked again. Fragments such as $C_9H_{10}^+$ (118 amu) and $C_{10}H_{12}^+$ (132 amu) can be formed from the hydrogen chain end via the elimination of a phenyl. The simultaneous or subsequent loss of one H atom would yield fragments $C_9H_9^+$ (117 amu) and $C_{10}H_{11}^+$ (131 amu), which are more stable as ions. The neighbor $C_{10}H_9^+$ (129 amu) is probably due in part to the rearrangement of $C_{10}H_{11}^+$ by hydrogen loss. The intense $C_{15}H_{13}^+$ (193 amu) may also be produced from the hydrogen chain end, assuming a loss of H_2 from $C_{15}H_{15}^+$. In contrast, $C_{12}H_{17}^+$ (161 amu) obviously arises from the butyl chain end via direct scission of the backbone after the first phenyl. The formation pathways of $C_{13}H_{11}^+$ (167 amu) and of $C_{14}H_{13}^+$ (181 amu) are less evident and involve important rearrangements with respect to the initial structure of the molecule.

Finally, for submonolayers of PS oligomers on transition metals, distributions of higher mass fragments and parentlike ions are also observed. They are shown in the last frame of Figure 5. The parentlike ions have the form $[M + Me]^+$, where M is the organic molecule and Me is the metal atom, and the fragments are lighter hydrocarbon chain segments associated to a metal particle. A striking feature of the distributions of unfragmented parent molecules is that they mirror quite accurately the real molecular weight distribution of the molecules on the surface (within 10% error).[57] That is, both the sputtering and ionization probabilities of these large molecular aggregates are almost independent of the organic molecule mass, which can differ by 1 order of magnitude in a single distribution. Although the ion formation processes might be different, it is interesting to note that metal-cationized PS oligomers are observed in matrix-assisted laser desorption ionization (MALDI[58,59]) and electrospray ionization (ESI[58,60]) mass spectrometries. In SIMS, the KEDs of these oligomers clearly indicate a collision-induced ejection mechanism, as opposed to a thermal desorption.[12]

(b) Calculated Mass Spectrum. The calculated mass spectrum, corrected to exclude polyatomic species that might decompose on the time scale of the experiment, has been shown in Figure 3b. It is important to note that this spectrum excludes unstable species but does not include unimolecular dissociation *products*. In the very low mass range, the organic peak pattern is dominated by intense H, H_2, C, CH, C_2H, and especially C_2H_2 fragments. Acetylene is indeed a very stable molecule, and it has been observed with a high intensity in the calculated spectra of ethylidyne,[23] alkanethiolate,[25] and benzene.[26] In the range 0−120 amu, besides the small hydrocarbon and silver peaks, the spectrum shows a number of less intense but more characteristic peaks that mirror the molecular structure of the butyl-terminated PS tetramer molecule. These fall roughly into two classes, namely, aromatic and aliphatic species. The first series is dominated by C_6H_5, the phenyl side group of polystyrene, and includes smaller fragments (C_3H_2, C_4H_3, and C_5H_3) as well as larger chain segments (C_7H_7, C_8H_9, and C_9H_9). The second series is constituted by fragments whose structure evokes the butylchain end (C_2H_5, C_3H_6, C_4H_9, and C_5H_{11}). Before a detailed discussion of the origin of these species, it is worth remarking that the same two series of peaks are observed in the experimental spectrum of Figure 5. In the high mass region beyond 400 amu of Figure 3b, there is a very intense peak for the entire molecule (474 amu), accompanied by weak peaks corresponding to large fragments. There is also a small contribution of Ag-cationized molecules at 582 amu. In the intermediate mass range, there are a series of fragments also arising from the scission of the main chain at different places. Fragments at 118, 132, 145, 195, and 209 amu include the phenyl chain end, whereas fragments at 161, 175, and 188 amu include the butyl chain end. Some of them have an equivalent in the experimental spectrum (118, 132, 145, 161, and 195 amu). Not surprisingly, polycyclic hydrocarbons are insignificant in the calculated spectrum, because their formation requires considerable rearrangement of the original fragments.

As indicated by the detailed description presented above, the mass spectra obtained in the SIMS experiment and in the MD simulation have many common features. Most of the characteristic fragment ions observed below 120 amu have a homologue in the calculated spectrum, and entire molecules are sputtered in both cases. It is remarkable considering the important approximations underlying molecular dynamics as were performed in this study. For instance, no ionization effects, no thermal effects, and no products of metastable decay are included. Nevertheless, there are a few striking differences that need to be addressed.

First, it has been remarked in previous studies that the MD calculated spectra showed large hydrocarbon peaks at even masses that were much weaker in the experimental spectra.[25] In the low-mass range of the PS calculated spectrum (Figure 3), such peaks occur, for instance, at 26 (C_2H_2), 38 (C_3H_2), 52 (C_4H_4), and 90 amu (C_7H_6). This can be explained by the different stabilities of hydrocarbon ions as compared to neutral molecules. While an even mass neutral hydrocarbon molecule is very stable because all of its electrons are paired, the even mass hydrocarbon ion is significantly less stable and more reactive than the corresponding odd mass one because one of its electrons is unpaired. Although significant exceptions exist in SIMS, these radical ions appearing at even masses often constitute much weaker peaks than their even-electron counterparts at odd masses. For instance, the bulk PS spectrum obtained after single-photon ionization of the sputtered neutral fragments exhibits large peaks at 50, 52, 78, and 104 amu[61] which are much weaker in the corresponding SIMS spectrum.[53]

Second, it is very interesting that the experimentally observed polycyclic hydrocarbons, which might be the result of unimolecular dissociation processes, are weak or absent from the calculated spectrum. In this respect, it is tempting to suggest that the number of large excited species excluded from the calculated mass spectrum of Figure 3b decay on their way to the detector, possibly giving rise to polycyclic hydrocarbons. For example, we have already mentioned the metastable decay of C_9H_9 into the bicyclic idenyllium radical predicted by extended time calculations (section 3.1). To check this idea further, calculations up to 1 μs should be made with a representative set of ejected fragments. Nevertheless, even with unlimited CPU time, the question concerning the appropriateness of the potential would still prevent a quantitative interpretation of the results, not to mention limitations related to the stability of the numerical integration and round-off errors.

Another important difference concerns the parentlike ions. Although many Ag-cationized oligomers and virtually no single molecules are detected in the experiment (in contrast with other aromatic hydrocarbons such as anthracene,[62] coronene,[63] dibenzanthracene,[12] and tetraphenylnaphthalene[12]), the calculated spectrum exhibits a very intense molecular peak and a weak $[M + Ag]$ peak. The reason for the absence of ionized parent molecules in the experimental spectrum is not precisely known. In a previous work,[12] it has been proposed that the energy needed to ionize such a molecule was higher than that required

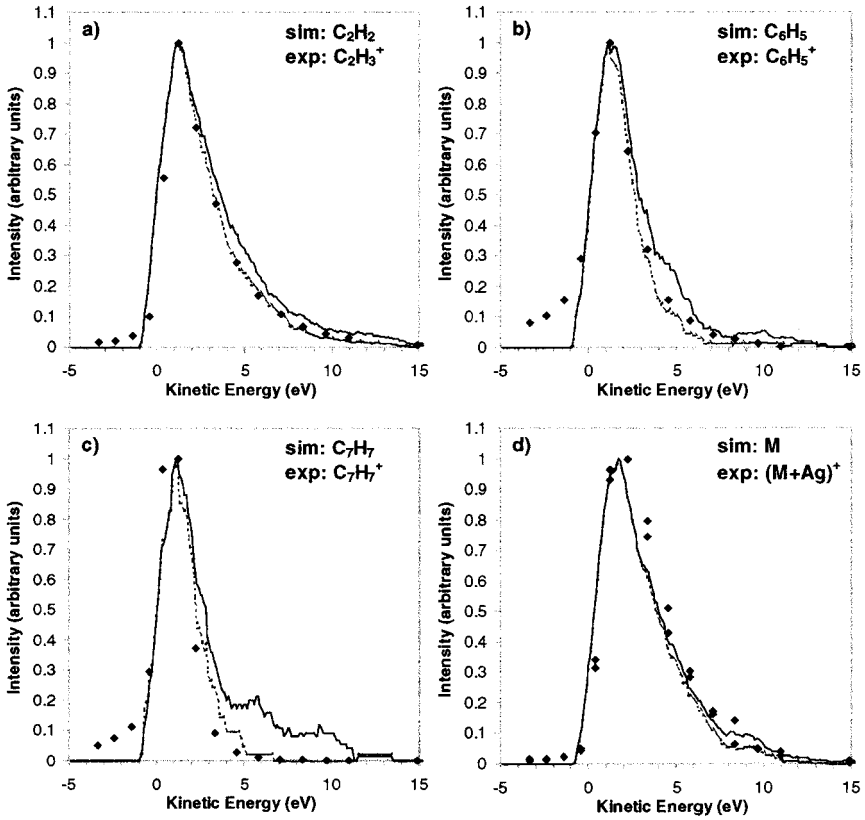

Figure 6. Kinetic energy distributions of selected fragments sputtered from *sec*-butyl-terminated PS tetramers adsorbed on Ag{111} under 500 eV Ar atom bombardment. Full lines correspond to the KEDs including all of the fragments with the selected formulas and dashed lines to the KEDs obtained for fragments with internal energies of less than the calculated threshold for dissociation. Experimental KEDs are indicated by black diamonds. The formulas of the fragments are indicated in the top right corner of each frame.

for fragmentation. In turn, the association of the departing molecule with a silver ion would be a less energetic and more efficient pathway to produce a cation. Also, there is little doubt that neutral parents are produced in the sputtering experiment, as a corollary to the significant yield of $[M + Ag]^+$ species. Hence, the possibility to eject large organic molecules as observed in the simulation is not questioned but rather the ability to ionize them in the experiment. Furthermore, the relatively low yield of Ag-cationized molecules in the simulation can be easily explained. Indeed, the Ag−C and Ag−H potentials which realistically describe the binding of benzene to silver surfaces[26] are not expected to describe adequately the binding of silver atoms, much less silver ions to similar molecules in the vacuum. In turn, the calculated Ag−benzene binding energy in the vacuum is much lower than that measured for the real Ag^+−benzene system (0.3 versus 1.7 eV,[64] respectively). This argument, valid for benzene, holds for polystyrene too. To overcome this limitation, a new kind of potential has been proposed recently, and it has been proved successful to account for the interaction of sulfur with both gold single atoms and surfaces.[25] A similar modification is not developed for the silver−hydrocarbon system, because the particular interaction between silver atoms and aromatic hydrocarbon is not expected to affect the formation of other species sputtered from PS. Nonetheless, this weakness of the model must be kept in mind for the interpretation of the results.

The comparison of the experimental and calculated mass spectra was the first step to estimate the quality of the MD model. Besides sputtering yields, the kinetic energy distributions of the sputtered fragments are expected to tell more about the physics of the ejection. Therefore, the comparison of such quantities should constitute a more stringent test of the model. The comparison of kinetic energy distributions is the next step of our verification procedure.

3.3. Kinetic Energy Distributions. *(a) Characteristic Fragments.* The kinetic energy distribution of sputtered particles constitutes an important parameter to help identify the mechanism responsible for emission. In addition, the KED of sputtered molecular ions can be measured with various experimental setups in a well-established manner. As described in ref 12, the KEDs of hydrocarbon parent and fragment ions sputtered from PS oligomers cast on silver have been measured using a time of flight spectrometer. In this instrument, the secondary ions are given a high kinetic energy of 3 keV before being 90° deflected by a first electrostatic analyzer (ESA). The ESA transforms the initial energy distribution into a spatial distribution, so that well-resolved energy windows can be filtered by placing a narrow slit at the following crossover of the secondary ion beam. The theoretical energy resolution of the apparatus is 1.5 eV, but previous measurements showed that the full width half-maximum (fwhm) of the measured KEDs never fell below 2 eV, indicating a slightly larger value for the actual resolution (estimated passband: 2 ± 0.3 eV). To compare with the experimental results, energy distributions derived from the simulation are then calculated with the same 2 eV energy resolution. As shown in ref 14 using poly(ethylene terephthalate) targets and in ref 26 for benzene adsorbed on silver, the influence of the primary beam on the KED of limited size molecular species appears negligible, therefore allowing us to compare 500 eV simulation with 15 keV experiments. The validity of such a comparison in the case of larger molecules is discussed in detail in section 3.5.

The calculated and experimental KEDs of several fragments of PS are shown in Figure 6. The phenyl radical (C_6H_5) is the

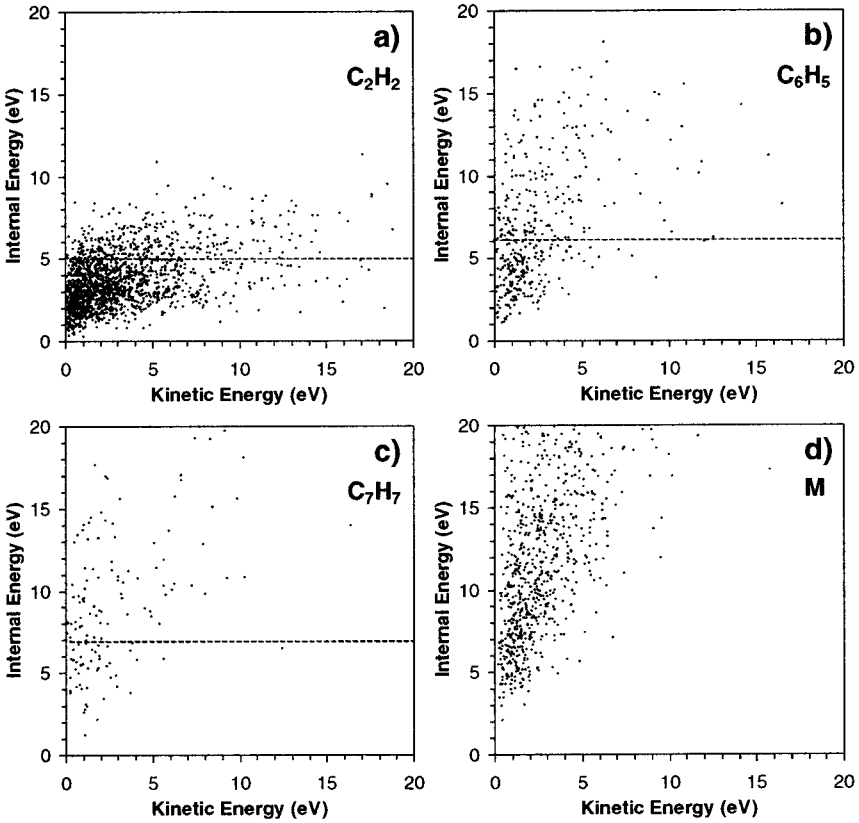

Figure 7. Scatter plots correlating the internal energies of selected secondary species with their kinetic energies. The formulas of the fragments are indicated in the top right corner of each frame. The horizontal lines indicate the value of the calculated threshold for dissociation.

most intense fragment in the range 30−120 amu of the calculated spectrum and a very characteristic fragment in SIMS (Figure 6b). In the experiment, it is thought to arise from the phenyl side groups of PS. Similarly, C_7H_7 has been chosen because it is the more intense peak in the experimental spectrum of high molecular weight PS as well as PS oligomers (Figure 6c). To check the influence of the fragment size on the KEDs, a smaller fragment, C_2H_3 (C_2H_2), has been chosen (Figure 6a). Again, $C_2H_3^+$ constitutes an intense peak in the very low mass range of the SIMS spectrum (Figure 5). Because the number of C_2H_3 produced in the simulation is too low to obtain a satisfactory distribution, the experimental $C_2H_3^+$ is compared to its stable neutral counterpart, C_2H_2, which is very intense in the calculated spectrum. The fact that the smooth distribution of C_2H_2 averages the noisy distribution of C_2H_3 in the simulation justifies this comparison. Finally, the distributions of sputtered parent species are compared in Figure 6d.

The agreement between the simulation and the experiment is satisfactory, as shown by the solid lines in Figure 6, even if the calculated distributions are not corrected to exclude unstable species. For large fragments such as C_6H_5 and C_7H_7, however, the high-energy contribution is more intense in the simulation. Instead, if the internal energy filter is applied (dashed lines in Figure 6), the agreement becomes remarkable, especially if one remembers that the energy resolution of the experiment is not accurately known and that metastable decay reaction products are not taken into account. For the smaller C_2H_2 species, the internal energy filtered and the total calculated KEDs nearly merge, because most of these species are stable relative to our dissociation criterion. The calculated distribution of entire PS tetramers is very similar to those of Ag-cationized PS oligomers in SIMS.[12] Again, the influence of the correction on the calculated distributions is negligible because the dissociation threshold is very high and only excludes a small fraction of the ejected species.

Concerning the physics of the emission, several important conclusions can be drawn from the results presented in Figure 6. First, they confirm that characteristic fragments of PS like C_6H_5 and C_7H_7 can be sputtered by collisional mechanisms. Moreover, the good match of the KEDs suggests that collisional interaction is the predominant mechanism to explain the emission of these ionic fragments. In contrast, a major thermal contribution would shift the distributions toward lower energies. Second, it has been reported previously that the decrease of the mean kinetic energy with increasing fragment size was a general trend for hydrocarbon fragments.[10] The simulation indicates the two different sources of this reduction. The first important factor is the nature of the collisional interaction itself, as indicated by the comparison between the distributions of C_7H_7 and C_2H_2 before correction. The second factor that reduces significantly the average kinetic energy of intermediate-size fragments such as C_7H_7 is the internal energy-dependent dissociation of excited species, as shown by the narrower distribution after correction. In contrast, the weaker influence of the energy threshold for higher mass species, along with the different nature of the emission mechanism (see section 3.4), accounts for the broader distribution of the parentlike ions.[12]

(b) Connection between Kinetic and Internal Energies. It is intriguing that the depletion of the high-energy tails after correction is more pronounced for intermediate-size species than for very small fragments and large chain segments (Figure 6). To understand this characteristic behavior, observed in the simulation as well as the experiment, it is useful to see how the internal and kinetic energies are connected for selected molecular species. This relation is plotted in Figure 7 for the species considered in Figure 6. The horizontal lines indicate the value

of the dissociation threshold for the corresponding fragments. In general, the internal and kinetic energies are correlated and an average ratio R = internal energy/kinetic energy can be obtained using a linear regression to fit the data. A similar correlation was observed previously for ejected benzene molecules and the average ratio was close to 1.[26] Similarly, a linear correlation has been predicted in analytical models.[15,65,66] Nevertheless, in contrast with simple analytical predictions, the correlations of Figure 7 are far from perfect, as witnessed by the important dispersion of the data. This dispersion is due to the variety of mechanisms that give rise to a given fragment.

The existence of a correlation between kinetic and internal energies accounts for the selective depletion of the high-energy tail of the KEDs after the exclusion of the more excited species. Now, the more subtle increase of the influence of the correction on the KEDs when going from very small hydrocarbons to intermediate-size fragments and then its reduction for larger species can be tentatively explained. In the very low mass range below 20−30 amu, an important fraction of the ejected species is stable because their internal energy is lower than the threshold; thus, the KEDs are not strongly influenced by the correction. With increasing fragment mass up to 200−300 amu, the average internal energy of the fragments increases more than the threshold for dissociation. Therefore, a larger fraction of energetic fragments is excluded, and the effect of the correction becomes important. In contrast, beyond 200−300 amu, the dissociation threshold increases faster than the average internal energy, so that the effect of the correction finally becomes insignificant for entire PS tetramers.

The saturation of the average internal energy in the high mass region (Figure 4b) is related to the nature of the collisional interaction. In these bombardment conditions, the total energy transferred to the departing species may not be higher than 40−45 eV, as shown in section 3.4. Long chain segments and entire molecules, with a large number of vibrational modes, can accumulate important amounts of internal energy and still survive to the detector. A completely different behavior would be observed with a constant internal energy threshold. In particular, the high-energy tail of the KED would be strongly depleted for entire molecules, and it would no longer mirror the experimental distributions.

In Figure 7, R is close to 5 for the entire molecule, showing that the fraction of energy transferred to the internal modes of the molecule is much higher than the fraction inducing the center-of-mass motion. Even for the phenyl radical (C_6H_5), which is similar to benzene in mass and structure, R equals 3. It is smaller than one for short fragments, e.g., between $^1/_3$ and $^1/_2$ for acetylene (C_2H_2). In general then, R is correlated to the size of the ejected species, and the larger polyatomic particles receive more vibrational and rotational energy during the emission process. The high value of R found for the PS tetramer in comparison with benzene[26] is probably due to the interplay of several factors. The first factor is the larger size of the PS tetramer. Indeed, in the first stages of the interaction, recoil silver atoms only impart momentum to localized parts of the molecule, and the other parts remain at rest. Therefore, the ejected molecules should be strongly distorted, and eventually they should carry a high vibrational energy. The second factor is the greater stiffness of the benzene molecule, having a ring structure and stronger bonds, that should increase the propensity to react as a whole entity, compared to the weaker and less rigid, σ-bonded PS backbone. The third factor is the different binding energies of the two molecules to the silver surface, i.e., ~2.3 eV for polystyrene and ~0.4 eV for benzene. The relatively high average internal energy of the phenyl radical with respect to benzene[26] is probably due to the different bond strengths of the precursor on the surface and/or to the different collision processes needed to knock it off. For comparison, the C−C bond retaining the phenyl ring is close to 5 eV, which is 1 order of magnitude greater than the binding energy of physisorbed benzene. Breaking this covalent bond to sputter the phenyl then should require more energy and, in turn, induce more vibrational excitation.

(c) H-Deficient Fragments. The agreement between calculated and measured KEDs in Figure 6 is very good. However, if the experimental KEDs of C_2H^+ and $C_7H_5^+$ were compared to that calculated for C_2H and C_7H_5, a discrepancy would appear. As a general trend, the KEDs of species differing only by the number of hydrogen atoms are similar in the simulation. In contrast, it has been shown that the width of the KEDs *increases* with a decrease in the number of hydrogen atoms in the experiment.[11] To explain the formation of these dehydrogenated ions in the experiment, the internal-energy-dependent fragmentation of excited parents has been invoked. In this hypothesis, hydrogen-deficient fragments arise from the dissociation of excited precursor like ions soon after their emission. As the kinetic and internal energies are correlated, the fragmentation by hydrogen loss should lead to a depletion of the high-energy tail of the precursor KED and to a much broader distribution for the hydrogen-deficient daughter molecules.[15]

If one looks at the trajectories in the simulation, dissociation reactions such as these rarely occur within the investigated time scale. In addition, it has been shown with other systems that the hydrogen-deficient fragment peaks observed in the experiments were often weaker or absent in the calculated mass spectra.[25] Late dissociation of the precursorlike ions by H_2 loss in the vacuum has then been proposed to explain the formation of these hydrogen-deficient fragments and their absence in the simulation.

It is remarkable that these interpretations, suggested on the two independent grounds of KED measurements and previous MD simulations, appear consistent and complementary. Moreover, H and H_2 losses have recently been shown to be a favorable decomposition channel for sputtered hydrocarbon ions at times larger than 1 ns in the experiment[13] and shorter than 100 ps in the simulation (section 3.1). Hence, upon merging of our interpretations, molecular species which are hydrogen-deficient or strongly fragmented with respect to the PS structure should be formed mainly by fast metastable decay in the vacuum or by a combination of metastable decay and direct emission. Because the direct emission is the only accessible mechanism using MD simulation, the observed KEDs mirror exclusively this contribution, ignoring the significant fraction of similar daughters produced in the vacuum. This explains why the KEDs of dehydrogenated ions are significantly different in the experimental and calculated results.

According to our refined explanation, the calculated internal-energy-resolved KEDs, i.e., the KEDs corresponding to increasing internal energy passbands (0−5 and 5−15 eV), should reflect the change observed with increasing unsaturation in the experiment. The internal-energy-resolved KEDs of C_7H_7 are displayed in Figure 8a. With decreasing internal energy, the KEDs become narrower and their high-energy tails become steeper. As expected, the experimental KEDs of C_7H_y cations with $y = 5-7$ show that a similar effect occurs for fragments with increasing number of H atoms (Figure 8b). Both effects are even more pronounced for smaller and less characteristic fragments.

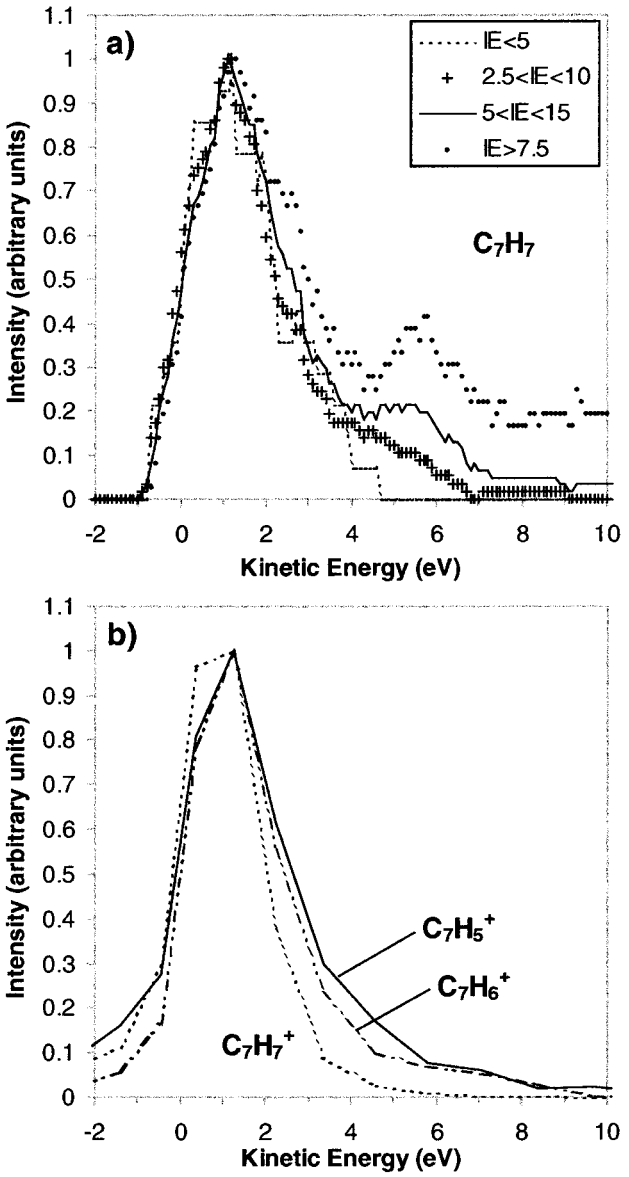

Figure 8. (a) Calculated internal energy resolved kinetic energy distributions of C_7H_7. (b) Experimental kinetic energy distributions of $C_7H_5^+$, $C_7H_6^+$, and $C_7H_7^+$.

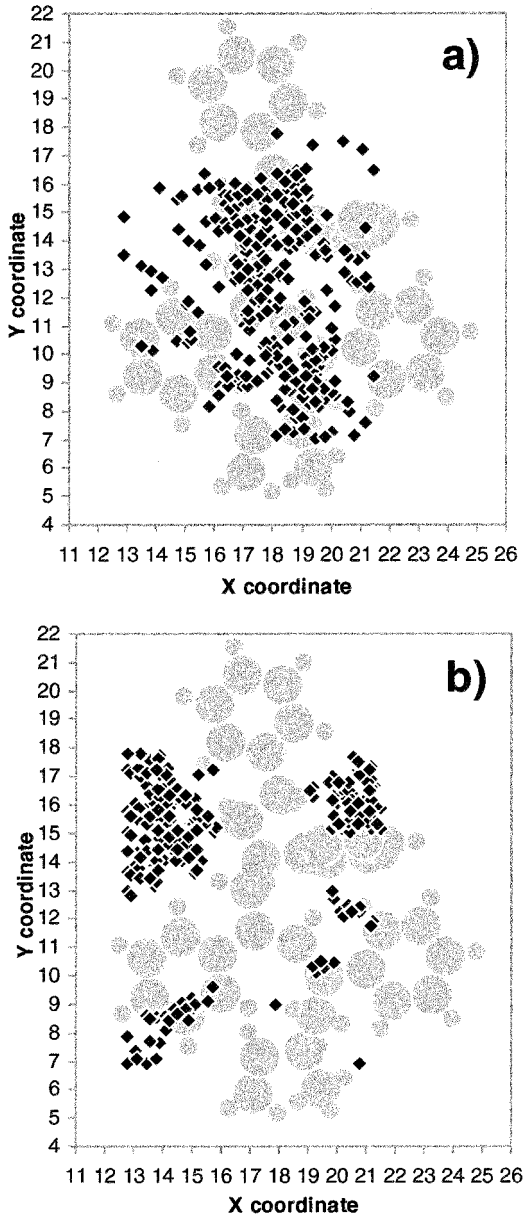

Figure 9. Scatter plot of the impact points of the primary Ar atom on the sample surface. The impact points are depicted by black diamonds and the central PS tetramer by gray spheres. (a) Impact points inducing the emission of C_6H_5 fragments. (b) Impact points inducing the emission of the entire PS tetramer.

3.4. Emission mechanisms. *(a) Influence of the Impact Point.* In addition to statistics that can be compared to experimental data, the simulation provides a microscopic view of the emission process. To show the sequence of events that lead to the ejection, the fragment and parent particle emissions are illustrated by selected snapshots of the MD. Before particular examples are shown, the connection between the position of the primary impact points and the position of the molecular species to be sputtered provides general insight into the nature of the mechanisms.

Figure 9 maps the positions of the C and H atoms belonging to the central PS tetramer of Figure 1, along with primary Ar aiming points that are efficient for the sputtering of various molecular species. The aiming points that induce the ejection of a phenyl ring (C_6H_5) are plotted in Figure 9a. They are concentrated in the close proximity of carbon atoms and, more precisely, along the backbone of the molecule. Conversely, very few trajectories that aim at the bare silver areas induce the ejection of C_6H_5. This behavior is observed for most fragments in the low mass range of the calculated spectrum. This indicates that the emission of fragments is mainly induced by the close interaction between the primary Ar atom and the organic molecule, that is, before the Ar atom reaches the silver substrate. Thus, this very early interaction precedes the development of collision cascades in the substrate. The ejection of characteristic fragments by this mechanism is exemplified in this section. In contrast, the emission of the unfragmented central molecule is possible, but the primary particle must impact directly the silver substrate, as shown in Figure 9b. Many of the efficient aiming points are indeed concentrated in bare substrate regions.

The distributions of distances between the aiming point and the center of mass of the ejected particles have been calculated for species sputtered from the five organic molecules. The distributions are shown in Figure 10a for sputtered species covering the whole mass range of the mass spectrum, i.e., atomic carbon, C_2H_2, C_6H_5, and the entire molecule. The very narrow distribution of C atom distances indicates that the ejection of carbon atoms is mainly due to their direct interaction with the primary particle. For the other species, the position of the

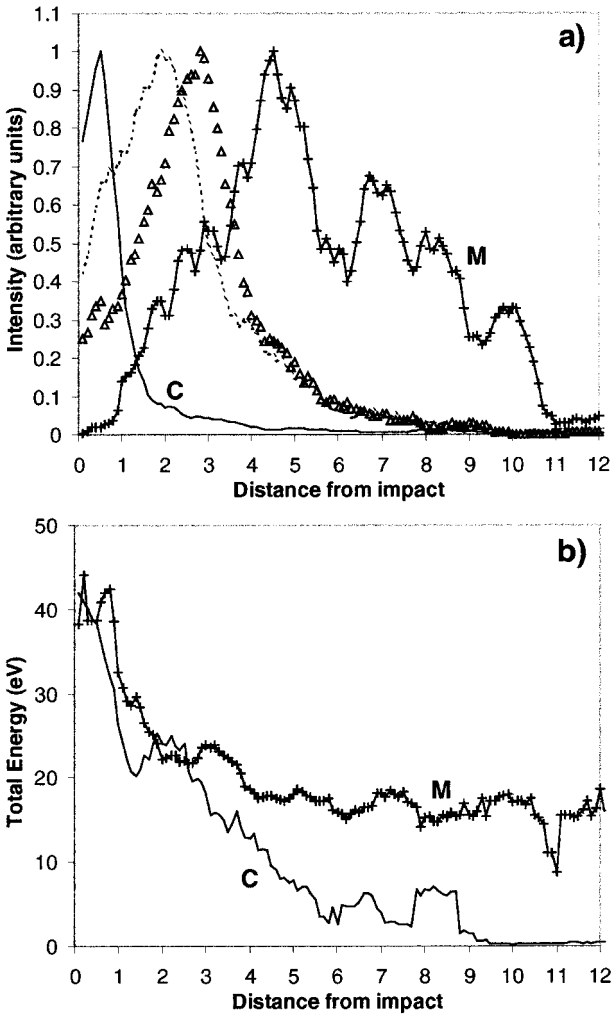

Figure 10. (a) Yield of sputtered species as a function of the distance between their center of mass and the impact point of the primary Ar atom on the surface. Carbon atoms are indicated by a full line, C_2H_2 by a dashed line, C_6H_5 by open triangles and the entire PS tetramer by a line with plus signs. (b) Sum of the kinetic and internal energies per sputtered species as a function of the distance between their center of mass and the impact point of the primary Ar atom on the surface. Carbon atoms are indicated by a full line and the entire PS tetramer by a line with plus signs.

maximum and the width of the distributions increase with increasing molecule size. The maxima occur at 2 Å for C_2H_2, 3 Å for C_6H_5, and 5 Å for the molecule. These distances are quite short relative to the size, $\sim 20 \times 15$ Å, of the PS tetramer. This result suggests that the ejection of fragments is mostly induced by the collision of the primary Ar atom with a close neighbor atom in the molecule. In addition, the entire PS tetramer is ejected more efficiently when the primary impact on the bare silver happens close to the molecule and the ejection becomes already negligible beyond 10 Å. In parallel, Figure 10b shows the average *total* energy transferred to the sputtered C atoms and PS tetramers as a function of the distance from the primary particle impact. This value indicates how the energy of the impact is distributed at the surface. Below 3 Å, the two curves match and the average energy decreases from 40−45 to 15−20 eV. Beyond 3 Å, the curve of the carbon tends to go to zero, while that of the molecule forms a plateau. Figure 10b shows that, in contrast with small fragments and atoms, large sputtered molecules always store a certain amount of energy during the emission process, independent of the distance from the impact point. This total energy threshold is dominated by internal vibrational and rotational energy.

The behavior depicted in Figure 10 evokes the "precursor" model suggested by Benninghoven.[67] To explain the emission of both entire molecules and fragmented species, he first proposed a concept using the average distribution of the energy in the surface region. According to this concept, fragments are produced close to the impact point, where the deposited energy is high, while unfragmented molecules are ejected from farther away, where the energy remains under the threshold for fragmentation. Experimental results in favor of this model have been obtained in the fields of kiloelectronvolt[68] and megaelectronvolt[69] ion bombardment of organic molecules. The distributions of Figure 10, depicting the yield and average energy of the ejected species as a function of the distance from the impact point, support this prediction too. Figure 10a shows that intact molecules are preferentially emitted at some distance from the primary impact and that the average distance of maximum emission for fragments increases with their size. In addition, the average energy around the impact point, indicated by the total energy of the sputtered species, decreases quickly with increasing distance (Figure 10b). Benninghoven's concept that relies on the collision cascade theory, however, does not foresee the predominant effect of the interaction between the primary atom and the organic molecule in the ejection processes. In contrast, the initial scission of the organic molecule by the primary particle has been proposed by Leggett and Vickerman as a precondition to fragment ejection from polymers.[55] Based on the MD results, the remainder of this section addresses in detail the emission mechanisms of the most characteristic fragments and entire molecules sputtered from PS tetramers adsorbed on Ag.

(b) Fragments. Very small organic fragments may be formed by multiple channels. For instance, the simulation results indicate that C_2H_2 can be produced by C−C bond scissions either in any of the four phenyl side groups (without hydrogen loss) or in the backbone. In the latter case, the excess hydrogen atom may have been kicked off before the C−C scissions occur or may be released in a subsequent collision with other segments of the molecule, or even by very fast unimolecular dissociation as shown in ref 23. Finally, the formation of some C_2H_2 molecules includes hydrogen exchange or hydrogen capture, via interaction with the rest of the molecule. The variety of mechanisms and their multiple combinations show that a single characteristic ejection scenario or fragmentation channel cannot be identified for fragments such as C_2H_2 or smaller. On the other hand, this explains their very high yield in the MD simulation.

In contrast, the origin of slightly larger PS characteristic fragments, including C_3H_2, C_3H_3, C_4H_3, C_4H_4, C_5H_4, C_5H_5, and C_6H_5, is easier to track. The vast majority of these species come from the four phenyl side groups of the molecule. For the small fragments with three or four carbon atoms, the ejection is often caused by the collision of the primary argon atom with the phenyl ring itself, leading to its fast fragmentation. For larger fragments with five or six carbons, the emission may rather be induced by the collision with the first carbon neighbor of the phenyl in the backbone.

The statistics concerning the fragments with six and more carbon atoms, truly characteristic of the PS structure, are displayed in Table 2. In parallel, Figure 1 helps to locate the main origin of these fragments in the molecule. As mentioned before, below 110 amu, the fragment size is not the predominant factor that influences the fraction of stable species (Table 2,

TABLE 2: Statistics of the Characteristic Fragments Sputtered from the PS Tetramer/Ag{111} Sample under a 500 eV Argon Atom Bombardment

	no. of fragments	fraction of stable fragments (%)	from the central/ aimed PS (%)	from inside the chain (not ends) (%)	hydrogen capture/ exchange/ loss (%)
C_6H_4	170	45	94	74	L: 100
C_6H_5	386	52	96	69	E: 11
C_6H_6	94	21	97	65	C: 99
C_7H_6	152	24	97	64	L: 36
C_7H_7	136	38	96	25	C + E: 35
C_8H_8	107	17	93	50	L: 50
C_8H_9	131	49	91	7	C + E: 9
C_9H_9	25	8	100	92	L: 100
C_9H_{10}	36	22	92	69	E: 44

column 3). For a given size, the percentage may vary strongly with the number of hydrogen atoms in the fragment. For instance, it depends on whether the fragment is formed via a single C−C bond breaking (C_6H_5, C_8H_9), a hydrogen capture mechanism (C_6H_6), or multiple bond scissions (C_6H_4, C_7H_6, C_8H_8, and C_9H_9). Column 4 confirms that more than 90% of the fragments come from the only molecule that can be hit directly by the primary projectile, in the center of the silver crystal surface.

Among the fragments with six carbons, the phenyl radicals (C_6H_5) dominate. They are mostly formed via a direct scission of the C−C bond linking a phenyl to the PS backbone. Nevertheless, it is interesting to note that more than 10% of these fragments undergo hydrogen exchange with neighbor carbon atoms. In the mass spectrum of Figure 3, the phenyl radical is surrounded by two satellite peaks, the less intense C_6H_6 and C_6H_4 fragments. While the benzene molecules are exclusively formed by hydrogen capture, the C_6H_4 fragments form via hydrogen loss from the phenyl side groups.

Larger unsaturated fragments such as C_7H_6, C_7H_7, C_8H_8, C_8H_9, C_9H_8, and C_9H_9 always include a phenyl ring and a portion of the backbone (see Figure 1 and Table 2). Among these fragments, C_7H_7 and C_8H_8 are particularly interesting from the viewpoint of the SIMS analysis because they are the most characteristic of the PS repeat unit (C_8H_8). Besides the emission from the H chain end, proper to the case of short oligomers, one-fourth of the C_7H_7 and half of the C_8H_8 are sputtered from inside the chain, as a result of two C−C bonds breaking in the backbone of the PS tetramers. These emission mechanisms are thus expected to occur in the case of high molecular weight PS too. The case of C_7H_7 is particularly complex, because its formation from inside the chain requires a hydrogen capture.[56,70] In this respect, experiments with selectively deuterated statistical and block copolymers have shown the short range of the H transfer.[71,72] Our results confirm this trend, as shown hereafter. In addition to H capture, the simulation shows that hydrogen-exchange reactions also affect a significant fraction of the C_7H_7 sputtered from the chain end. In most cases, C_7H_7 has the benzyl and not the tropylium structure. In sharp contrast with C_7H_7, only a tiny fraction of C_8H_9 is ejected from inside the molecule via hydrogen capture, confirming the very special status of C_7H_7. Beyond 110 amu, a very small fraction of the fragments that are characteristic of both PS oligomers and high molecular weight PS is stable. Except C_9H_9 and C_9H_{10}, the fragments observed in this mass range, listed in section 3.2, are generally formed via a single bond scission in the PS tetramer backbone.

The emission of fragments containing six, seven, and eight carbon atoms is illustrated in Figure 11. Although this example has been selected among many others because it combines several interesting fragments in the same trajectory, each of the described channels is representative of an important emission mechanism for the corresponding fragment. The three frames show top views of the central PS tetramer at different time steps in the simulation. At 20 fs, the impinging argon atom collides almost simultaneously with two carbon atoms in the middle of the molecular backbone. The first carbon atom, initially bonded to the phenyl side group, is violently pushed downward into

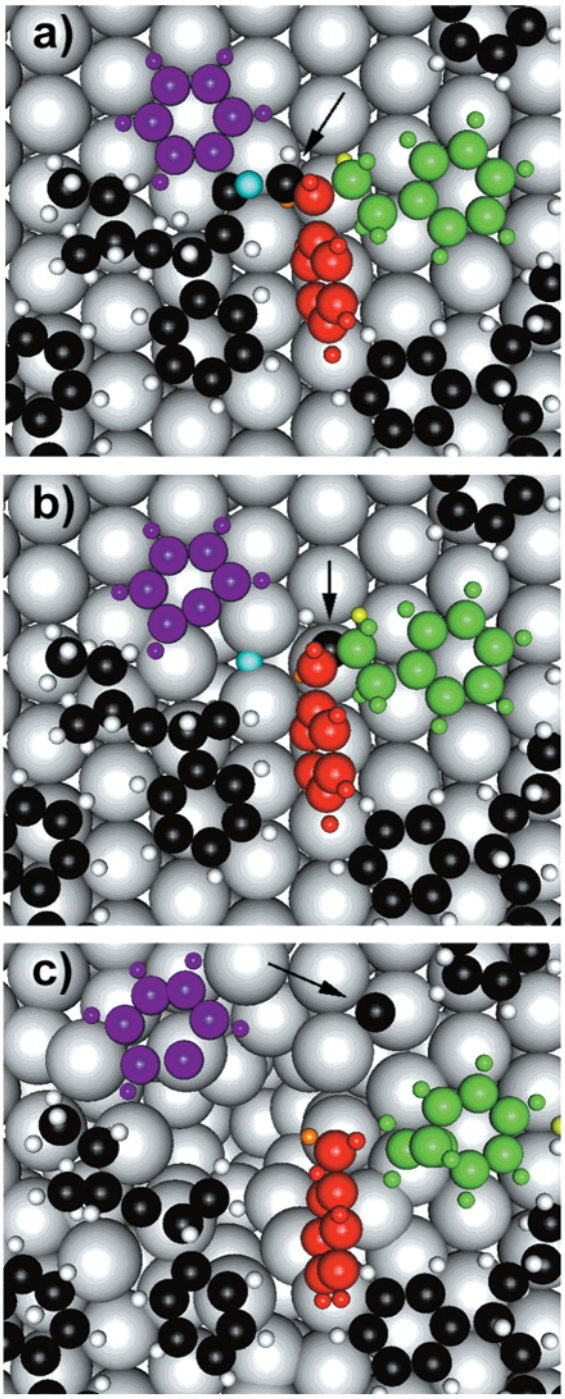

Figure 11. Mechanistic view of the formation of characteristic fragments sputtered from PS tetramers. The primary Ar atom is colored in cyan. The three important fragments discussed in the text are colored in purple (C_6H_5), red (C_7H_7), and green (C_8H_8). The H atom that eventually forms the C_7H_7 fragment is orange. The H atom that is ejected from the nascent C_8H_8 is lime green. The C atom that induces a second bond scission in the PS tetramer backbone is indicated by an arrow. The three frames show the time evolution of the event: (a) 20 fs; (b) 30 fs; (c) 110 fs.

the silver substrate, which allows for the release of a C_6H_5 fragment (purple). The second recoil carbon atom moves laterally above the silver layer and along the molecule, as shown by the arrow. At 30 fs, after being reflected by a silver atom, it hits another carbon atom of the molecule, which leads to a second C−C scission in the backbone and, eventually, to the emission of C_7H_7 (red) and C_8H_8 (green). To form C_7H_7, one of the hydrogen atoms (orange) released by the laterally moving carbon is captured by the nascent C_7H_6. In addition, the interaction of the moving carbon atom with the chain end induces the ejection of another hydrogen atom (lime green), producing C_8H_8. After 110 fs, six fragments are moving toward the vacuum including one H atom, one C atom, three stable molecular fragments—C_6H_5 (purple), C_7H_7 (red), and C_8H_8 (green)—and one large unstable species—$C_{13}H_{18}$ (black). Alternative and slightly different fragmentation pathways lead to the emission of the other important fragments listed in Table 2.

In summary, what is the general picture of fragment ejection provided by the MD simulation? Is there any implication for the SIMS analysis of organic molecule and polymer fragments? First, the simulation indicates that the most characteristic fragments of PS may be produced by a direct emission process. Except hydrogen exchange or capture, recombination reactions between two molecules or between fragments of a molecule are negligible, with our system constituted of isolated and relatively flat molecules. The collisionally induced fragments are thus representative of the chemical structure of the sample. Second, the fragmentation of PS tetramers is mainly induced by the early interaction with the primary argon atom. The close collision with a carbon atom of the backbone, resulting in its implantation in the substrate, is an efficient way to release neighbor fragments with a low internal energy excess. To produce stable fragments from inside the chain, a second bond scission is required. It is often caused by a very small energetic fragment or atom also set in motion by the primary interaction with the argon atom (moving carbon in Figure 11). This mechanism is particularly interesting in SIMS of polymers because it provides insights into the emission of fragments from high molecular weight molecules, where two bond-breaking events are required to produce large fragments. The role of the interaction with the primary atom and with laterally moving species in the fragmentation has been evidenced in previous papers for vertical alkyls[23] and alkanethiol chains[25] too. Third, the 100 ps calculations presented in section 3.1 suggest that unimolecular dissociation reactions might be a significant source of characteristic ions; e.g., C_7H_7 may be formed by the reaction $C_9H_9 \rightarrow C_7H_7 + C_2H_2$ (Table 1). On the other hand, the good match of the experimental and calculated KEDs indicates that there is no need to invoke thermally induced reactions on the surface to explain the formation of characteristic fragments such as C_7H_7 or C_8H_8 from inside the PS tetramer chain. Finally, although the agreement between the calculated and experimental spectra of PS oligomers is generally good, polycyclic hydrocarbons are not produced in the simulation. To explain this discrepancy, we propose that unimolecular dissociation reactions play a major role, so that polycyclic hydrocarbons form during the flight to the detector by the relaxation of excited parent species, i.e., via hydrogen loss and structural rearrangement. Similar hydrogen loss reactions are also likely to occur in the case of alkyl[23] and alkanethiol chains,[25] and they have been observed in the sputtering of hydrocarbon polymers.[13]

(c) Parent Molecules. In general, the analysis of the trajectories indicates that the ejection of entire PS tetramers is induced by upward moving silver atoms belonging to the top layer of the crystal, as a result of the collision cascades in the solid. Sequential and even quasi-simultaneous interactions with several silver atoms, as well as quasi-one atom collisions, are frequent. There is no major trend emerging from the simulation results. As was the case for flat benzene[26] and biphenyl molecules,[27] the ejection may be induced by the interaction with either a single or several silver atoms. For the sake of clarity, the ejection scenarios can be tentatively divided into these two classes. First, the ejection can be induced by a single, energetic silver atom, with more than 5−10 eV of kinetic energy. Second, the molecule liftoff may be the result of interaction with two, or more, moving silver atoms (cooperative uplifting). The one atom collision scenario, as well as the interaction with several energetic silver atoms that have completely uncorrelated velocity vectors, is likely to produce molecules with a large amount of vibrational motion (high R). In contrast, the smooth cooperative uplifting by several silver atoms with a limited kinetic energy and correlated velocity vectors is the most efficient to produce cool molecules with a relatively high kinetic energy (low R), as observed in ToF-SIMS experiments. An example of each scenario, i.e., quasi-one atom collision and cooperative uplifting, is discussed in the following paragraph.

Figure 12 shows snapshots from the MD illustrating two distinct events involving the same molecule (bottom left molecule in Figure 2). Frame a is common to the two considered events and shows a side view of the bottom left side of the sample, as shown in Figure 2, before starting the action. Frames b and c show successive time steps of the first trajectory, whereas frames d−f correspond to the second trajectory. In the first event, frame b shows that the molecule is pushed by a single silver atom moving upward at approximately 300 fs. This collision transfers sufficient momentum to eject the molecule. After 1300 fs, the molecule has left the surface and flies toward the vacuum (frame c). In this case, the shape and orientation of the molecule have been significantly altered by vibrational and rotational motion. The molecule has a kinetic energy of 1.9 eV and an internal energy of 11.1 eV at the end of the event.

A different scenario unfolds in the second trajectory. Frame d indicates that the action starts at the approximate time of 200 fs, with the soft collective motion of the silver atoms underneath the PS molecule. Of note is that the fast silver atom leaving at the bottom right of frames d and e does not impart its momentum to the molecule. At 300 fs, the gentle, cooperative uplifting of the molecule is underway. The movie indicates that at least five silver atoms act together to lift up the PS tetramer. Frame f shows a later view of the ejected molecule with an accompanying silver atom. It is remarkable that the orientation of the molecule in the vacuum is nearly unchanged, suggesting this time that the vibrational and rotational excitations are low. Indeed, the detailed analysis of the sputtered species confirms that this molecule has 6.7 eV of kinetic energy and 7.1 eV of internal energy at the end of the trajectory. Hence, this mechanism produces a stable molecule with a relatively high kinetic energy.

Although the total energy transferred to the departing molecule is very similar in the two examples illustrated above (13.0 and 13.8 eV, respectively), the partitioning of this energy in the internal and translational modes is completely different. The first molecule is slow and internally excited, whereas the second is faster but relatively cool. These two extreme cases explain the important dispersion in Figure 7d.

To gain a better understanding of these emission processes, the energy of the top layer silver atoms has been monitored as a function of time. Figure 13 shows two top views of the surface

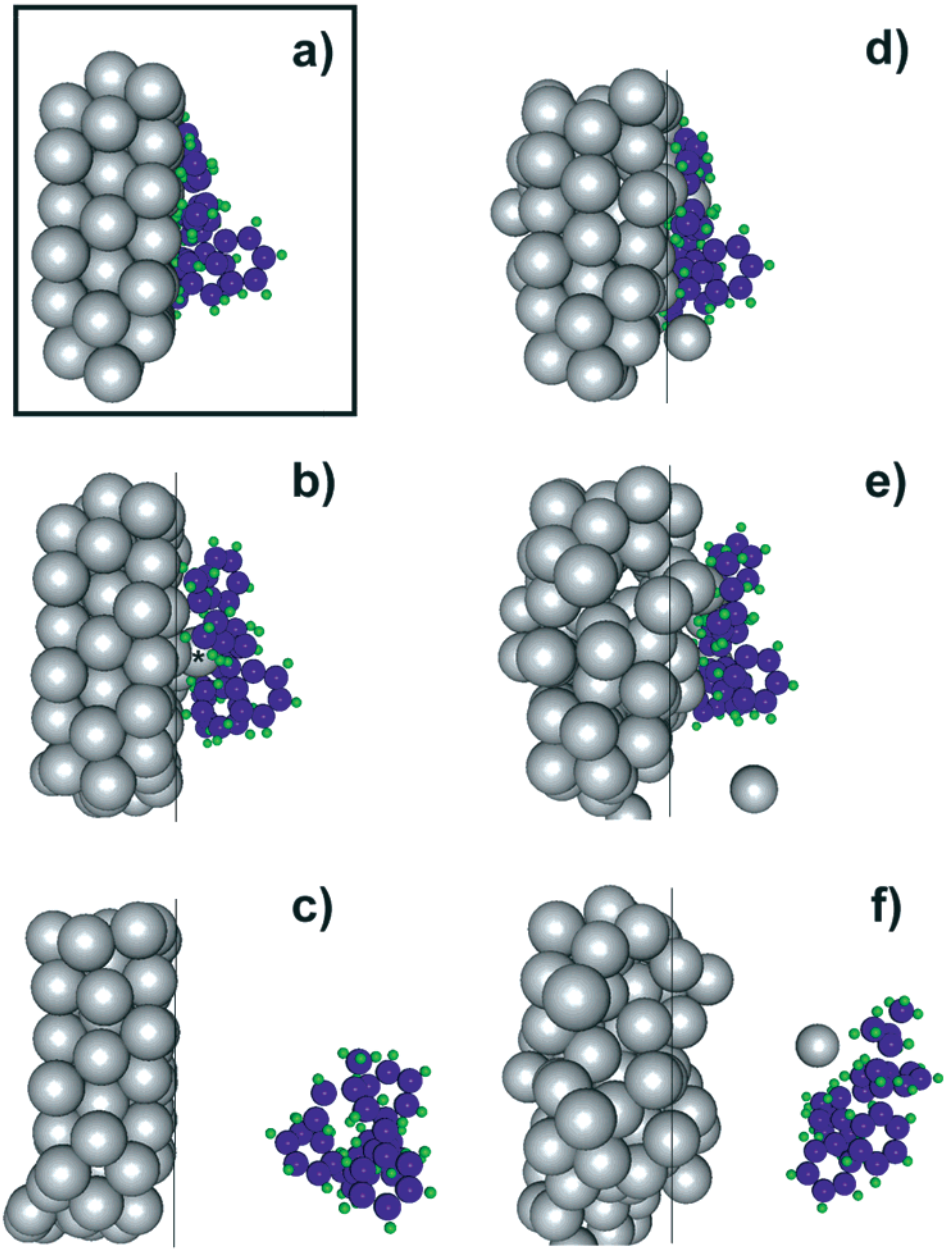

Figure 12. Two different ejection mechanisms for entire PS tetramers. Frames b and c correspond to the first event and frames d−f to the second event. Frame a shows the initial situation of the PS tetramer on the surface, common to both events. The other frames show the time evolution of the two events. First event: (b) 300 fs; (c) 1300 fs. Second event: (d) 200 fs; (e) 300 fs; (f) 800 fs.

silver layer corresponding to the two trajectories depicted above. The initial positions of the atoms are indicated by black dots. The shape of the bottom left molecule is delimited by black lines (see Figure 2 for correspondence). The energy of the silver atoms moving upward is indicated by the size and hue of the spheres. The small diamonds correspond to silver atoms moving downward. Figure 13a shows the action preceding the molecule emission in the first trajectory (Figure 12 b,c). After 117 fs, a collision cascade reaches the PS tetramer, and the fourth silver atom in the fourth row from the bottom hits the center of the molecule with a kinetic energy of 12.5 eV, causing ejection of the molecule. Another atom with a kinetic energy of 3 eV interacts with the molecule at the same time. Simultaneously, the four downward-moving silver atoms probably weaken the attraction between the molecule and the silver substrate. The localized interaction with the very fast silver atom explains the high internal energy of the molecule after ejection. Indeed, the tetramer reacts somewhat like a car bumper, absorbing most of the collision energy in its deformation. Figure 13b shows the energy of the top silver atoms after 158 fs in the second trajectory previously described (Figure 12d−f). As noticed before, the very energetic silver atom (15.4 eV) at the fifth position in the second row from the bottom leaves the surface without interacting with the molecule. On the other hand, four silver atoms with an energy close to 2.5 eV and five others with a lower energy between 0.5 and 1.5 eV interact simultaneously with different parts of the molecule. The result is a smooth cooperative uplifting of the entire molecule.

In analytical models, the idea of correlated motion of the target atoms has been developed to explain the emission of large metallic clusters and biomolecules that are unlikely to arise from single collisions or from statistical recombination processes. In this context, large polyatomic species are thought to emerge from regions where many atoms are set in motion with nearly parallel and equal momenta. Collective mechanisms have been described with different premises in the *gas-flow*,[73,74] *shock*

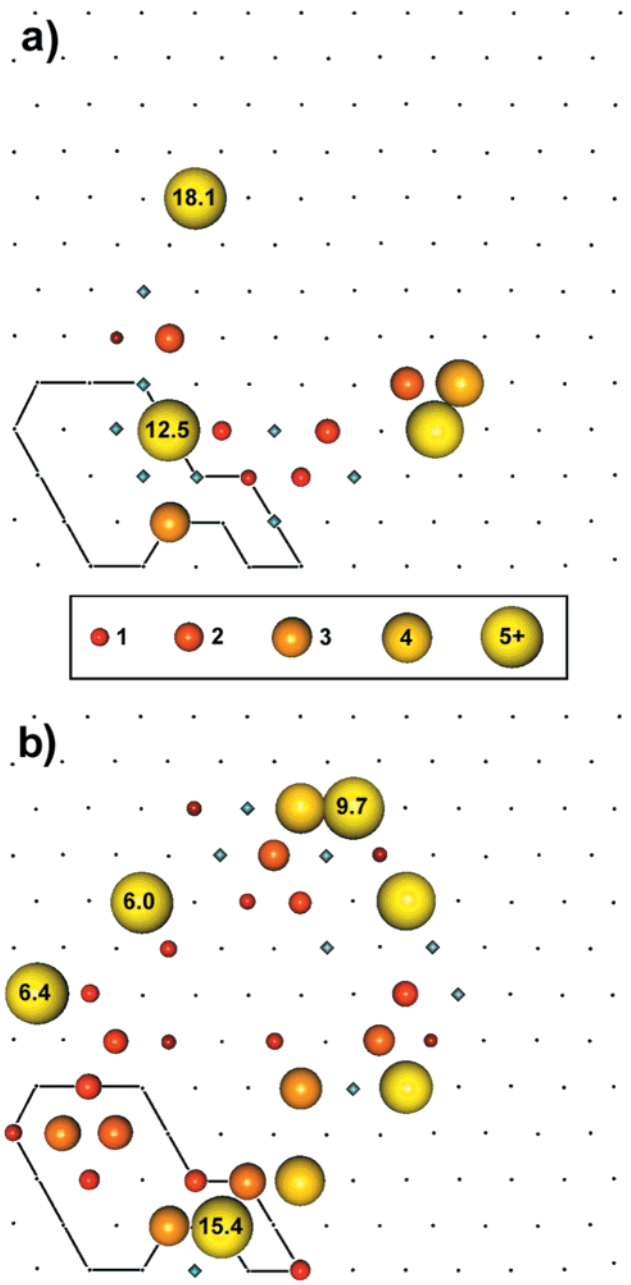

Figure 13. Picture of the kinetic energy of the first layer Ag atoms at the time they interact with the PS tetramer in the two events illustrated in Figure 12. The initial position of the silver atoms on the surface is indicated by black dots. Ag atoms moving downward are depicted by cyan diamonds. The kinetic energy of the upward-moving Ag atoms is represented by red to yellow spheres with different sizes and tones. The scale is in electronvolts. (a) 117 fs; (b) 158 fs.

wave[75,76] and *pressure pulse*[77] models. They were invoked in the case of kiloelectronvolt atom bombardment of biomolecules[78,79] and condensed amorphous rare gases.[80] Collective motions—as opposed to binary collisions—undoubtedly occur in the silver substrate of our sample, as illustrated by the protrusions of Figure 12e and 12f. The correlation of momentum among the silver atoms, observed under 500 eV argon bombardment, induces the ejection of fast but cool molecules that are not expected to undergo unimolecular dissociation after emission. However, neither massive flow of material nor shock waves were observed in our simulations. In particular, the collective motion of Figure 12 is the logical termination of a cooled collision cascade intersecting the surface plane, when the energy of the atoms is so low that they all "touch" each other.

3.5. Influence of the Primary Particle Energy. To check the influence of the primary beam energy, a larger crystal has been bombarded by 5 keV argon atoms. On average, the calculation time for one trajectory at 5 keV is 1 order of magnitude greater than that at 500 eV. Therefore, only 100 trajectories were calculated. Although this number of events is insufficient to compare mass spectra or energy distributions, several interesting observations can be drawn from the simulation results.

First, in agreement with the increase of the stopping power, the yields of silver atoms and entire molecules are much higher at 5 keV (Ag, 4.6; M, 1.3) than at 500 eV (Ag, 1.5; M, 0.2). The increase is more pronounced for entire molecules. The fractions of stable molecules, however, are similar (5 keV, 93%; 500 eV, 94%). Again, because of the low number of runs, the 5 keV numbers have larger statistical uncertainty.

As observed in the 500 eV simulation, the direct collision between the argon atom and the target molecule is very efficient to produce low-mass fragments, and intact molecule emission is induced by collision cascades in the silver substrate. Nevertheless, under 5 keV argon bombardment, the distance between the impact point and the sputtered molecule can be much larger than that indicated in Figure 10 for the 500 eV bombardment conditions. As expected, the primary ion energy influences directly the size of the excited area at the surface and presumably the distribution of energy as a function of the distance from the impact point (Figure 10b). In the case of cooperative uplifting, the ejection might be sensitive to the size of the excited region at the surface. Indeed, even for statistical processes, if the area in which substrate atoms receive upward momentum grows, the probability to observe a correlated effect for a molecule that is larger or equivalent in size to the perturbed area increases too. Our simulations show that the size of the excited area at the surface may well be larger than the size of PS tetramers even at 500 eV. This might explain why the effect of the primary particle energy on the emission of entire molecules is not pronounced in our system. However, the emission of larger molecules, such as heavier oligomers or biomolecules, might be influenced more strongly.

In contrast to the 500 eV bombardment, some trajectories provoke a very significant perturbation of the sample. In these cases, a large amount of the primary atom energy is released by hard collisions in a small volume, generating several energetic collision cascades. The overlapping of these cascades causes the collective motion of a large number of atoms in the substrate. If this region of collective motion intersects the surface, a large number of silver atoms and PS molecules, as well as silver (Ag_n) and organometallic clusters (M + Ag, M + Ag_2, M + Ag_3) may be sputtered. Such a large sputtering event is shown in Figure 14. In this case, collision cascades evolve and overlap in the top left corner of the silver substrate. The massive ejection of silver atoms and clusters leads to the temporary formation of a wide crater, indicated by arrows. At the end of this trajectory, 2 [M + Ag_2] clusters, 5 entire molecules, 1 silver trimer, 2 silver dimers, and 18 silver atoms were counted. Although most of the ejected silver atoms come from the first layer, a significant number is sputtered from the second layer, and one is removed from the third layer. It is interesting to note that no organic *fragments* are produced in this event. Although moderate "collision cascade type" events dominate, such high action events are not rare. From the limited set of data, one can estimate that 1 out of 10 trajectories give

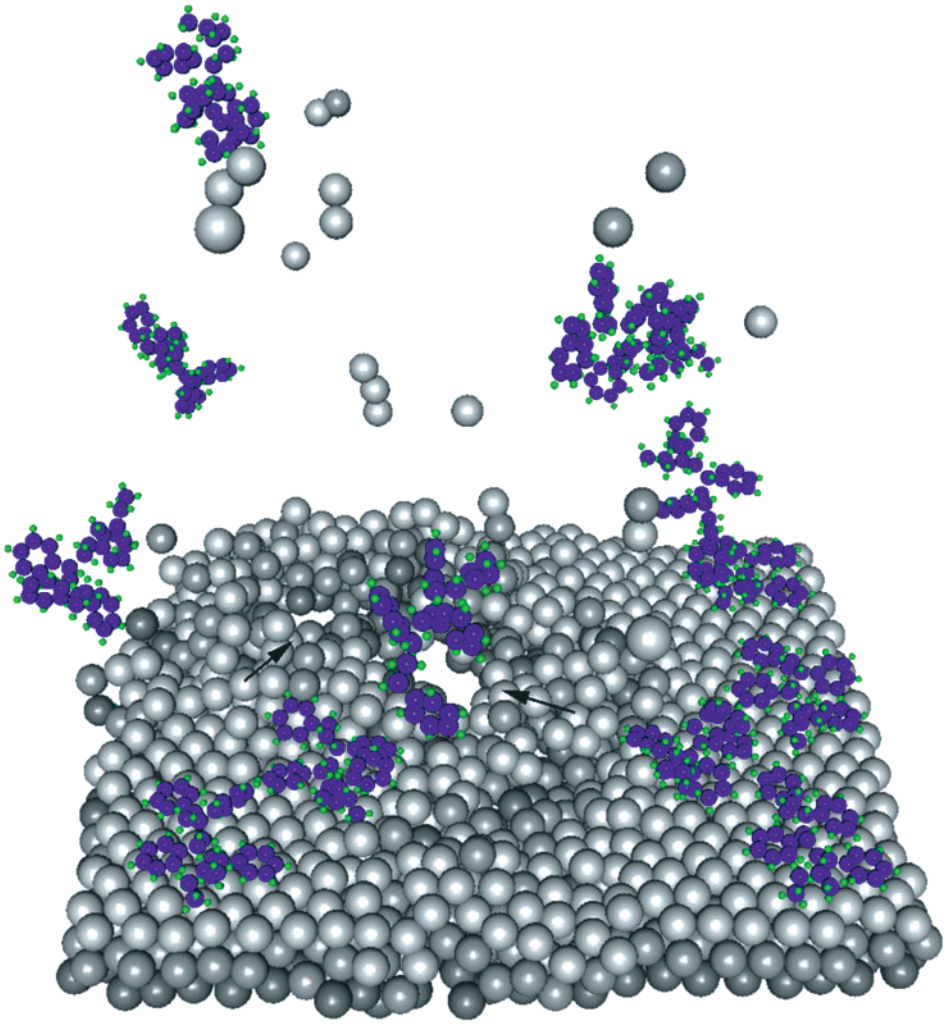

Figure 14. Mechanistic view of a large sputtering event induced in the large PS tetramer/Ag{111} sample by a 5 keV argon atom. The formation of a temporary crater is indicated by black arrows.

rise to similar events, characterized by a very high yield of substrate particles (more than 10) and/or organic molecules (4−5). Therefore, the impact of these events on the sputter yield cannot be neglected. In comparison with the 500 eV simulation, we have not found a clear indication that these events provide a more correlated momentum to neighbor silver atoms, appropriate to eject entire molecules with a very low internal energy/kinetic energy ratio. High action events (spikes) in metal crystals have been observed by several authors[81−84] and, in particular, they have been pointed out by Betz and co-workers to explain the emission of large clusters under kiloelectronvolt particle bombardment.[82,85,86] In our case, these "explosive" events appear less localized and do not produce such a highly correlated motion in the substrate.

4. Conclusions

The MD simulation of the kiloelectronvolt particle bombardment of a submonolayer of short PS oligomers on silver provides new insights into the emission mechanisms of fragments and parent molecules from large organic adsorbates. First, the calculated mass spectrum shows that many characteristic fragments of PS may be produced via a collisional interaction, including large C_6H_5, C_7H_7, and C_8H_8 as well as smaller fragments of the phenyl ring. The results indicate that a significant fraction of these species should be stable on the time scale of the experiment. In addition, the KEDs of these characteristic fragments agree well with the experiments realized with similar samples. At the microscopic level, the simulation results show that most of the fragments are the consequence of the direct interaction between the primary particle and the PS tetramer rather than the result of the collision cascades developing in the silver substrate. The interaction with the Ar atom is often followed by other C−C bond scissions caused by small moving atoms or fragments also produced in the initial collision. This two-step mechanism is very interesting for the case of high molecular weight polymers, because it leads to the emission of characteristic fragments from *inside* the hydrocarbon chain. In particular, it is interesting to note that a significant fraction of C_7H_7, the major peak of the experimental PS spectrum, is sputtered from inside the tetramer chain via two C−C bond scissions followed by a H atom capture. On the other hand, the polycyclic aromatic species observed in the range 120−200 amu of the experimental mass spectra are absent from the simulation. Unimolecular dissociation of large excited fragments in the vacuum might constitute a predominant formation channel for these ions.

Second, these MD simulations confirm that large organic adsorbates may be sputtered intact via collisional interactions. In general, the PS tetramers are lifted up by one or several silver atoms moving upward. While single and uncorrelated multiple collisions with substrate atoms are likely to give rise to ejected molecules with a high internal energy/kinetic energy ratio, the

cooperative uplifting by silver atoms with similar momenta may produce fast molecules with a limited internal excitation. In the 500 eV bombardment conditions, such cooperative mechanisms appear as cooled collision cascades intersecting the sample surface. Under 5 keV argon bombardment, besides isolated cascades, high action events occur in ~10% of the calculated trajectories. These events are characterized by a very high sputtering yield of both silver atoms and organic molecules. More than large-scale correlated motion, they appear as overlapping cascades inducing the simultaneous but uncoordinated motion of a large number of atoms in the metal substrate. The contribution of such events to the total yield of molecules is significant. Therefore, it should be possible to track their effects in the experiments and to check their influence on the kinetic energy of the sputtered species by adequate measurements using different primary beam energies. Because these events seem to produce few fragments, their implications on the yield and kinetic energy of such species should be minor. A more exhaustive MD study, including a larger number of runs at high energy, should help to unravel the genesis of these events. It should also predict their influence on the secondary particle yields and kinetic energies in a quantitative way.

Acknowledgment. The authors thank Nick Winograd, Kristin Krantzman, Chad Meserole, and Gareth Williams for helpful discussion and advice. The financial support of the National Science Foundation through the Chemistry Division, the CRIF program, and the MRI program is gratefully acknowledged by A.D. and B.J.G. Additional computational resources were provided in part by the IBM Selected University Resource Program and the Center for Academic Computing of The Pennsylvania State University. We are also indebted to the Center for Academic Computing staff for helping us use the IBM SP computer and for developing of a new graphics software for animation and presentation. X.V.E. is supported by the Belgian Interuniversity Attraction Pole Program (PAI-IUAP P4/10) on Reduced Dimensionality systems. The ToF-SIMS equipment was acquired with the support of the Région Wallonne and FRFC-Loterie Nationale of Belgium.

References and Notes

(1) Benninghoven, A.; Rüdenauer, F. G.; Werner, H. W. *Secondary Ion Mass Spectrometry*; Wiley: New York, 1987; p 699.
(2) *Secondary Ion Mass Spectrometry, SIMS XI Proceedings*; Gillen, G., Lareau, R., Bennett, J., Stevie, F., Eds.; Wiley: New York, 1998.
(3) Chatterjee, R.; Riederer, D. E.; Postawa, Z.; Winograd, N. *J. Phys. Chem. B* **1998**, *102*, 4176.
(4) Chatterjee, R.; Riederer, D. E.; Postawa, Z.; Winograd, N. *Rapid Commun. Mass Spectrom.* **1998**, *12*, 1226.
(5) Meserole, C. A.; Vandeweert, E.; Chatterjee, R.; Winograd, N.; Postawa, Z. *Appl. Surf. Sci.* **1999**, *141*, 339.
(6) Brown, A.; Vickerman, J. C. *Surf. Interface Anal.* **1986**, *8*, 75.
(7) Gilmore, I. S.; Seah, M. P. *Surf. Interface Anal.* **1995**, *23*, 191.
(8) Zubarev, R. A.; Abeywarna, U.; Hakansson, P.; Demirev, P.; Sundqvist, B. U. R. *Rapid Commun. Mass Spectrom.* **1996**, *10*, 1966.
(9) Delcorte, A.; Bertrand, P. *Nucl. Instrum. Methods B* **1996**, *115*, 246.
(10) Delcorte, A.; Segda, B. G.; Bertrand, P. *Surf. Sci.* **1997**, *381*, 18; *389*, 393.
(11) Delcorte, A.; Bertrand, P. *Nucl. Instrum. Methods B* **1998**, *135*, 430.
(12) Delcorte, A.; Bertrand, P. *Surf. Sci.* **1998**, *412/413*, 97.
(13) Delcorte, A.; Bertrand, P. *Int. J. Mass Spectrom.* **1999**, *184*, 217.
(14) Delcorte, A.; Vanden Eynde, X.; Bertrand, P.; Reich, D. F. *Int. J. Mass Spec.* **1999**, *189*, 133.
(15) Delcorte, A.; Bertrand, P. *Nucl. Instrum. Methods B* **1996**, *117*, 235.
(16) Sigmund, P. In *Sputtering by Particle Bombardment I*; Behrisch, R., Ed.; Springer-Verlag: Berlin, 1981; p 9.
(17) Garrison, B. J.; Delcorte, A.; Krantzman K. D. *Acc. Chem. Res.* **2000**, *35*, in press.
(18) Garrison, B. J. *J. Am. Chem. Soc.* **1982**, *104*, 6211.
(19) Garrison, B. J. *Int. J. Mass Spectrom. Ion Phys.* **1983**, *53*, 243.
(20) Taylor, R. S.; Brummel, C. L.; Winograd, N.; Garrison, B. J.; Vickerman, J. C. *Chem. Phys. Lett.* **1995**, *233*, 575.
(21) Taylor, R. S.; Garrison, B. J. *Chem. Phys. Lett.* **1994**, *230*, 495.
(22) Taylor, R. S.; Garrison, B. J. *J. Am. Chem. Soc.* **1994**, *116*, 4465.
(23) Taylor, R. S.; Garrison, B. J. *Langmuir* **1995**, *11*, 1220.
(24) Taylor, R. S.; Garrison, B. J. *Int. J. Mass Spectrom. Ion Processes* **1995**, *143*, 225.
(25) Liu, K. S. S.; Yong, C. W.; Garrison, B. J.; Vickerman, J. C. *J. Phys. Chem. B* **1999**, *103*, 3195.
(26) Chatterjee, R.; Postawa, Z.; Winograd, N.; Garrison, B. J. *J. Phys. Chem. B* **1999**, *103*, 151.
(27) Zaric, R.; Pearson, B.; Krantzman, K. D.; Garrison, B. J. G. *Int. J. Mass Spectrom. Ion Processes* **1998**, *174*, 155.
(28) Townes, J. A.; White, A. K.; Wiggins, E. N.; Krantzman, K. D. *J. Phys. Chem. A* **1999**, *103*, 4587.
(29) Kerford, M.; Webb, R. *Nucl. Instrum. Methods B* **1999**, *153*, 270.
(30) Webb, R.; Kerford, M.; Way, A.; Wilson, I. *Nucl. Instrum. Methods B* **1999**, *153*, 284.
(31) Beardmore, K.; Smith, R. *Nucl. Instrum. Methods B* **1995**, *102*, 223.
(32) Garrison, B. J.; Winograd, N.; Harrison, D. E., Jr. *J. Chem. Phys.* **1978**, *69*, 1440.
(33) Harrison, D. E., Jr. *CRC Crit. Rev. Solid State Mater. Sci.* **1988**, *14*, S1.
(34) Winograd, N.; Garrison, B. J. In *Ion Spectroscopies for Surface Analysis*; Czanderna, A. W., Hercules, D. M., Eds.; Plenum Press: New York, 1991; p 45.
(35) Garrison, B. J. *J. Chem. Soc. Rev.* **1992**, *21*, 155.
(36) Bernardo, D. N.; Bhatia, R.; Garrison, B. J. *Comput. Phys. Commun.* **1994**, *80*, 259.
(37) Stave, M. S.; Sanders, D. E.; Raeker, T. J.; DePristo, A. E. *J. Chem. Phys.* **1990**, *93*, 4413.
(38) Raeker, T. J.; DePristo, A. E. *Int. Rev. Phys. Chem.* **1991**, *10*, 1.
(39) Kelchner, C. L.; Halstead, D. M.; Perkins, L. S.; Wallace, N. M.; DePristo, A. E. *Surf. Sci.* **1994**, *310*, 425.
(40) Brenner, D. W. *Phys. Rev. B* **1990**, *42*, 9458.
(41) Brenner, D. W.; Harrison, J. A.; White, C. T.; Colton, R. J. *Thin Solid Films* **1991**, *206*, 220.
(42) Dudde, R.; Frank, K. H.; Koch, E. E. *Surf. Sci.* **1990**, *225*, 267
(43) Anderson, A. B.; McDevitt, M. R.; Urbach, F. L. *Surf. Sci.* **1984**, *146*, 80.
(44) Harrison, D. E., Jr.; Delaplain, C. B. *J. Appl. Phys.* **1976**, *47*, 2252.
(45) Wucher, A.; Garrison, B. J. *Phys. Rev. B* **1992**, *46*, 4855.
(46) Dzhemilev, N. K.; Goldenberg, A. M.; Veryovkin, I. V.; Verkhoturov, S. V. *Nucl. Instrum. Methods B* **1996**, *114*, 245.
(47) Kiermeier, A.; Kuhlewind, H.; Neusser, H. J.; Schlag, E. W. *J. Chem. Phys.* **1988**, *88*, 6182.
(48) Forst, W. *Theory of unimolecular reactions*; Academic Press: New York, 1973.
(49) Gotkis, Y.; Oleinikova, M.; Naor, M.; Lifshitz, C. *J. Phys. Chem.* **1993**, *97*, 12282.
(50) Kuhlewind, H.; Kiermeier, A.; Neusser, H. J. *J. Chem. Phys.* **1986**, *85*, 4427.
(51) Klippenstein, S. J.; Faulk, J. D.; Dunbar, R. C. *J. Chem. Phys.* **1993**, *98*, 243.
(52) Robinson, P. J.; Holbrook, K. A. *Unimolecular reactions*; Wiley: New York, 1972.
(53) *The Static SIMS Library*, Vickerman, J. C., Briggs, D., Henderson, A., Eds.; SurfaceSpectra: Manchester, 1997.
(54) Vanden Eynde, X.; Bertrand, P.; Jerome, R. *Macromolecules* **1997**, *30*, 6407.
(55) Leggett, G. J.; Vickerman, J. C. *Int. J. Mass Spectrom. Ion Processes* **1992**, *122*, 281.
(56) Chilkoti, A.; Castner, D. G.; Ratner, B. D. *Appl. Spectrosc.* **1991**, *45*, 209.
(57) Bletsos, I. V.; Hercules, D. M.; van Leyen, D.; Hagenhoff, B.; Niehuis, E.; Benninghoven, A. *Anal. Chem.* **1991**, *63*, 1953.
(58) Deery, M. J.; Jennings, K. R.; Jasieczek, C. B.; Haddleton, D. M.; Jackson, A. T.; Yates, H. T.; Scrivens, J. H. *Rapid Commun. Mass Spectrom.* **1997**, *11*, 57.
(59) Mowat, I. A.; Donovan, R. J. *Rapid Commun. Mass Spectrom.* **1995**, *9*, 82.
(60) Jasieczek, C. B.; Buzy, A.; Haddleton, D. M.; Jennings, K. R. *Rapid Commun. Mass Spectrom.* **1996**, *10*, 509.
(61) Pallix, J. B.; Schuhle, U.; Becker, C. H.; Huestis, D. L. *Anal. Chem.* **1989**, *61*, 805.
(62) Grade, H.; Cooks, R. G. *J. Am. Chem. Soc.* **1978**, *100*, 5615.
(63) Day, R. J.; Unger, S. E.; Cooks, R. G. *Anal. Chem.* **1980**, *52*, 557A.
(64) Ho, Y.-P.; Yang, Y.-C.; Klippenstein, S. J.; Dunbar, R. C. *J. Phys. Chem. A* **1997**, *101*, 3338.
(65) Snowdon, K. *Nucl. Instrum. Methods B* **1985**, *9*, 132.

(66) Sigmund, P.; Urbassek, H. M.; Matragrano, D. *Nucl. Instrum. Methods B* **1986**, *14*, 495.

(67) Benninghoven, A. In *Ion Formation From Organic Solids*; Benninghoven, A., Ed.; Series in Chemical Physics 25; Springer-Verlag: Berlin, 1983; p 77.

(68) Rading, D.; Kersting, R.; Benninghoven, A. In *Secondary Ion Mass Spectrometry, SIMS XI Proceedings*; Gillen, G., Lareau, R., Bennett, J., Stevie, F., Eds.; Wiley: New York, 1998; p 455.

(69) Papaleo, R. M.; Demirev, P.; Eriksson, J.; Hakansson, P.; Sundqvist, B. U. R.; Johnson, R. E. *Phys. Rev. Lett.* **1996**, *77*, 667.

(70) Vanden Eynde, X.; Reihs, K.; Bertrand, P. *Macromolecules* **1999**, *32*, 2925.

(71) Affrossman, S.; Hartshorne, M.; Jerome, R.; Pethrick, R. A.; Petitjean, S.; Vilar, M. R. *Macromolecules* **1993**, *26*, 6251.

(72) Affrossman, S.; Hartshorne, M.; Jerome, R.; Munro, H.; Pethrick, R. A.; Petitjean, S.; Vilar, M. R. *Macromolecules* **1993**, *26*, 5400.

(73) David, D. E.; Magnera, Th. F.; Tian, R.; Stulik, D.; Michl, J. *Nucl. Instrum. Methods B* **1986**, *14*, 378.

(74) Urbassek, H. M.; Michl, J. *Nucl. Instrum. Methods B* **1987**, *22*, 480.

(75) Bitenski, I. S.; Parilis, E. S. *Nucl. Instrum. Methods B* **1987**, *21*, 26.

(76) Bitenski, I. S. *Nucl. Instrum. Methods B* **1993**, *83*, 110.

(77) Johnson, R. E.; Sundqvist, B. U. R.; Hedin, A.; Fenyo, D. *Phys. Rev. B* **1989**, *40*, 49.

(78) Wong, S. S.; Rollgen, F. W. *Nucl. Instrum. Methods B* **1986**, *14*, 436.

(79) Sundqvist, B. U. R. *Nucl. Instrum. Methods B* **1990**, *48*, 517.

(80) Waldeer, K. T.; Urbassek, H. M. *Nucl. Instrum. Methods B* **1993**, *73*, 14.

(81) Ghaly, M.; Averback, R. S. *Phys. Rev. Lett.* **1994**, *72*, 364.

(82) Betz, G.; Husinsky, W. *Nucl. Instrum. Methods B* **1995**, *102*, 281.

(83) Urbassek, H. M. *Nucl. Instrum. Methods B* **1997**, *122*, 427.

(84) Shapiro, M. H.; Tombrello, T. A. *Nucl. Instrum. Methods B* **1999**, *152*, 221.

(85) Husinsky, W.; Betz, G. *Thin Solid Films* **1996**, *272*, 289.

(86) Betz, G.; Dandachi, C.; Husinsky, W. *Izv. Akad. Nauk: Ser. Fiz.* **1998**, *62*, 690.